

A *ROSAT* medium-sensitivity Galactic plane survey at $180^\circ < l < 280^\circ$

J. E. Morley,¹ K. R. Briggs,¹ J. P. Pye,^{1*} F. Favata,² G. Micela³ and S. Sciortino³

¹*X-Ray Astronomy Group, Department of Physics and Astronomy, University of Leicester, Leicester LE1 7RH*

²*Astrophysics Division, Space Science Department of ESA, ESTEC, Postbus 299, 2200 AG Noordwijk, the Netherlands*

³*Osservatorio Astronomico di Palermo, Piazza del Parlamento 1, 90134 Palermo, Italy*

Accepted 2001 May 11. Received 2001 April 30; in original form 2001 March 28

ABSTRACT

We have performed a moderately deep soft X-ray (0.1–2 keV) survey of the Galactic plane using pointed observations with the *ROSAT* Position Sensitive Proportional Counter (PSPC). The survey is more than an order of magnitude more sensitive than previous X-ray surveys near the Galactic plane. The data consist of nine fields each of ≈ 10 ks exposure, pointed at positions on or very close to the Galactic plane ($|b| < 0.3^\circ$) in the longitude range $180^\circ \leq l \leq 280^\circ$. This region has relatively low X-ray absorbing material out to distances of several hundred pc and presents fewer source-confusion problems than at other longitudes. The total sky area surveyed was 2.5 deg^2 ; this yielded 93 sources, 89 of which were detected in the ‘hard’ (0.4–2.0 keV) band. Nine sources were detected in both ‘soft’ (0.1–0.4 keV) and hard bands. In the hard band, the survey coverage is ≥ 90 per cent for sources brighter than $0.002 \text{ count s}^{-1}$ ($\sim 2 \times 10^{-14} \text{ erg cm}^{-2} \text{ s}^{-1}$), but falls steeply below this value, with the weakest sources being $\sim 0.001 \text{ count s}^{-1}$. The median limiting flux is $\approx 0.0013 \text{ count s}^{-1}$ ($\sim 1.3 \times 10^{-14} \text{ erg cm}^{-2} \text{ s}^{-1}$). There are 64 sources with hard-band count rates $> 0.002 \text{ count s}^{-1}$. We present the catalogue of X-ray sources and the number–flux relations ($\log N$ – $\log S$). Eighteen sources have possible identifications from the SIMBAD data base. We have searched the Tycho-2 and USNO-A2.0 catalogues to find all possible optical counterparts brighter than ~ 19 th magnitude, and attempt to classify these on the basis of $\log(f_X/f_{\text{opt}})$ versus optical colour diagrams and near-infrared photometry from the 2MASS Second Incremental Data Release. Hence, we have found the majority of these sources to be consistent with being late-type main-sequence stars, as previous studies have proposed from incompletely identified surveys. Comparison of the measured number–flux relations with predictions of Galactic (stellar) and extragalactic populations supports the view that the population of young stars in the plane is denser than previously thought.

Key words: catalogues – surveys – stars: late-type – Galaxy: stellar content – X-rays: general.

1 INTRODUCTION

Flux-limited surveys are important both in the study of source populations and in the identification of individual interesting objects. Using pointed observations from the *ROSAT* Position Sensitive Proportional Counter (PSPC), we present an X-ray source survey of the Galactic plane reaching a factor ~ 5 lower in flux than previous ‘Galactic plane’ surveys, namely the *Einstein* Galactic Plane Survey (EGPS; Hertz & Grindlay 1984, 1988) and the *ROSAT* Galactic Plane Survey (RGPS; Motch et al. 1991). The EGPS was a serendipitous source survey of Imaging Proportional Counter (IPC) fields at Galactic latitudes $|b| < 15^\circ$, covering a

total area of 275 deg^2 , and detecting 71 X-ray sources above a flux threshold of $\sim 2 \times 10^{-13} \text{ erg cm}^{-2} \text{ s}^{-1}$ in the energy band 0.15–4.5 keV. The median and 90 per cent coverage fluxes were $\approx 7 \times 10^{-13}$ and $\approx 2 \times 10^{-12} \text{ erg cm}^{-2} \text{ s}^{-1}$ respectively. The RGPS utilizes the *ROSAT* PSPC All-Sky Survey (RASS) data for $|b| < 20^\circ$, with a typical limiting flux of a few times $10^{-13} \text{ erg cm}^{-2} \text{ s}^{-1}$. Motch et al. (1991) have presented preliminary findings based on 225 sources detected in an area of $\approx 200 \text{ deg}^2$ in the longitude range $108^\circ < l < 155^\circ$. They have also presented analysis of a sample area covering 64.5 deg^2 centred on $l = 90^\circ$, $b = 0^\circ$, in which 128 sources were detected (Motch et al. 1997). The present survey, whilst covering a much smaller area of sky ($\approx 2.5 \text{ deg}^2$, $180^\circ \leq l \leq 280^\circ$, $|b| < 0.3^\circ$) than either the EGPS or RGPS, extends more than an order of magnitude deeper in flux,

*E-mail: pye@star.le.ac.uk

Table 1. Observation log. The H I column density through the Galaxy in each field position is from Stark et al. (1992). The H₂ column density through the Galaxy in each field position was found by applying a conversion factor (X-ratio) of $2.0 \times 10^{20} \text{ cm}^{-2}$ to the CO maps of Dame et al. (1987). The total hydrogen column density was calculated as $N_{\text{H}} = N_{\text{H I}} + 2 \times N_{\text{H}_2}$.

Field No.	Obs-Seq	RA (h m s)	Dec. (° ′ ″)	l (°)	b (°)	T_{exp} (ks)	$N_{\text{H I}}$	N_{H_2} (10^{20} cm^{-2})	N_{H}	Notes
1	900627	5 45 37.6	28 56 10.0	180.00	0.00	9.52	51.5	15.0	81.5	Gal. plane 1
2	200084	6 15 15.0	17 43 41.0	193.10	0.32	9.41	58.4	22.2	102.8	Target=G 104-27
3	900426	6 42 25.8	04 23 17.0	208.00	0.00	10.42	62.7	09.0	80.7	Gal. plane 2
4	900628	7 02 32.3	-05 23 54.0	219.00	0.00	8.59	67.7	11.2	90.1	Gal. plane 6
5	900380	7 18 29.0	-13 13 03.0	227.75	-0.13	18.68	61.0	09.7	80.4	Target=NGC 2359
6	900428	7 23 18.9	-15 08 33.0	230.00	0.00	9.84	69.2	09.7	88.6	Gal. plane 3
7	200049	7 24 40.1	-16 12 03.6	231.09	-0.21	8.66	74.3	06.7	87.7	Target=HD 58343
8	900427	8 10 02.8	-33 16 56.0	251.00	0.00	10.80	55.6	06.2	68.0	Gal. plane 4
9	400329	10 24 58.5	-57 47 00.5	284.39	-0.28	9.00	-	39.7	>79.4	Target=1E 102457

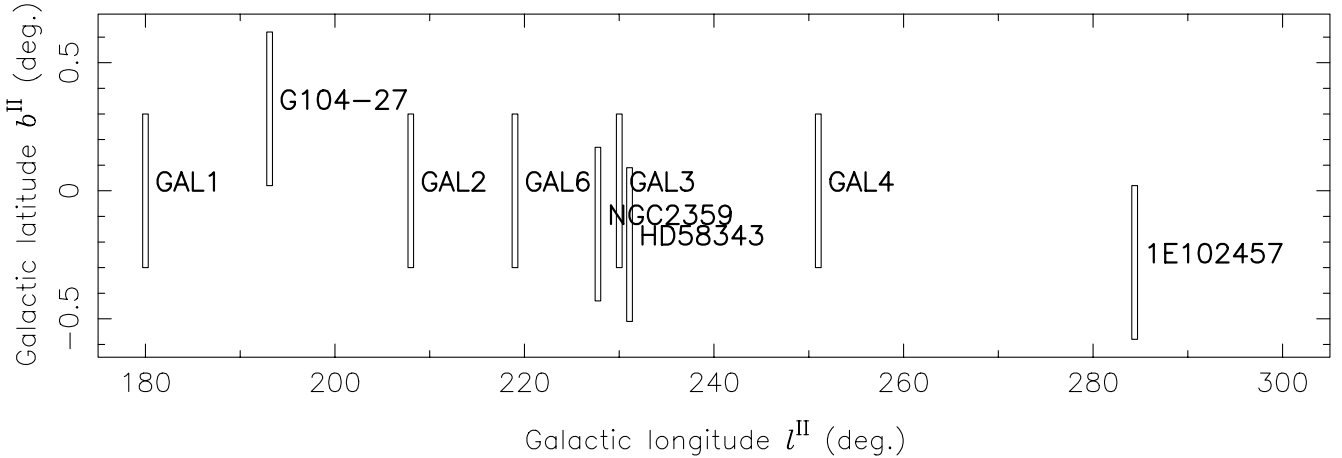


Figure 1. Relative positions of our fields along the plane. Each rectangle represents the longitudinal and latitudinal extent of the 18 arcmin radius field centre used in this survey.

to $\sim 10^{-14} \text{ erg cm}^{-2} \text{ s}^{-1}$, and has yielded 93 sources. Hence it complements well not only the EGPS and RGPS, but also *ROSAT* surveys at similar depths at high Galactic latitudes (e.g. Hasinger et al. 1993; Branduardi-Raymont et al. 1994; Boyle et al. 1995).

The longitude range selected for our survey has relatively low X-ray absorbing material out to distances of several hundred parsecs, and presents less confusion problems than at other longitudes. The restriction in latitude essentially removes scaleheight effects when attempting to interpret the spatial distribution of sources, since $|b| = 0^\circ.3$ corresponds to a height of only 5 pc off the plane at a distance from the Sun of 1 kpc. Previous surveys have typically found $\sim 80\text{--}90$ per cent of identified sources to be active coroneae, but left ~ 40 per cent of detected sources unidentified [although Motch et al. (1997) were able to identify 98 per cent of sources at a threshold of 0.03 PSPC count s^{-1} , $\approx 3 \times 10^{-13} \text{ erg cm}^{-2} \text{ s}^{-1}$]. We try to classify the sources in our (deeper) survey on the basis of X-ray to optical flux ratios and optical and near-infrared colours, to find the percentage that are consistent with being due to active coroneae.

The paper is organized as follows. In Section 2 we describe the data selection and the source-detection method. The determination of the number-flux relation is described in Section 3. Searches for optical counterparts are described in Section 4, and the methods used to classify these are detailed in Section 5. We compare our

results to model predictions in Section 6, and summarize them in Section 7.

2 OBSERVATIONS

2.1 Data selection

The survey used nine *ROSAT* (Trümper et al. 1991) PSPC (Pfeffermann et al. 1986) fields, each of ≈ 10 ks exposure, to sample the Galactic plane at longitudes from roughly 180° to 270° (the ‘third quadrant’).¹ A log of the observations is given in Table 1, while Fig. 1 shows the distribution of the fields on the sky. Five of the pointings (numbers 1, 3, 4, 6 and 8) were specifically performed for this programme, while the remaining four data sets were obtained from the archive.²

The target objects for these latter pointings are noted in Table 1. The field positions were selected to avoid molecular clouds, strong (≥ 0.2 PSPC count s^{-1}) known X-ray sources, bright stars and supernova remnants (SNRs), all of which might distort the survey. Each observation was required to have at least 8 ks exposure and to

¹ Some workers, e.g. Paresce (1984), refer to this as ‘quadrant 4’ or the ‘fourth quadrant’, while others, e.g. Frisch & York (1983), refer to it as ‘quadrant 3’ or the ‘third quadrant’. Here, we use the term ‘third quadrant’.

² These were the *only* archive data sets that fulfilled our criteria when the data selection for the project was made, in 1994 August. This remains true.

lie within 0.3° of the Galactic plane. A reasonably uniform sampling in longitude was achieved for $180^\circ \leq l \leq 250^\circ$. The gap in the region $260^\circ \leq l \leq 270^\circ$ is due to the Vela supernova remnant. In order to provide some sampling in this area, we included in our analysis field number 9, at $l \approx 284^\circ$. The most heavily sampled region is around $l \approx 230^\circ$, with fields 5, 6 and 7.

2.2 Source detection

Our analysis was restricted to the inner 18-arcmin radius of each field. This utilized the portion of the PSPC field of view (FOV) with the highest sensitivity and spatial resolution, and avoided potential problems due to shadowing by the window support structures. Those fields chosen from the archive also had the central 3.5-arcmin radius excluded from the analysis to prevent bias due to the central objects in these fields having been selected for their ‘interesting’ nature.³ Data intervals with poor aspect solutions (error ≥ 1 arcsec) or high anticoincidence rates (Master Veto Rate > 170) were also rejected.

Images were made in three photon energy bands: total (0.1–2.0 keV, PI channels 11–202), soft (0.1–0.4 keV, PI channels 11–42) and hard (0.4–2.0 keV, PI channels 43–202). Each image had dimensions of 200×200 pixel², with each pixel being 15×15 arcsec². Sources were detected using the point-source search program PSS.⁴ PSS required as input a data image and a corresponding background map.

The background map (one for each field and for each energy band) was constructed as follows. The average count rate was measured within the central 18-arcmin radius of an image. This was used for a preliminary PSS run. Detections made in this first run with a significance $> 4.0\sigma$ were then subtracted, and the resulting image smoothed using a 20×20 pixel² top-hat function. This was used as the background model for a second (and final) PSS run where detections were accepted as X-ray sources if they exceeded a significance of 4.5σ .

A total of 93 sources was detected; however, most of these (89) were also detected in the hard band and only 12 were detected in the soft band (three of which were detected in the soft band only). Hence most of our work has concentrated on the hard-band results, with consideration of the soft-band data where appropriate. The hard-band detections and the hard-band upper limits on the three soft-only detections are shown in Table 2. Sources detected in the soft band are shown in Table 3. Also shown in Table 3 are the hardness ratios for each source, defined as $HR = (H - S)/(H + S)$, where H and S are hard- and soft-band count rates respectively.

3 THE NUMBER–FLUX RELATION

The detection count-rate threshold is a function of exposure time and of position in each PSPC field since it depends on background level and vignetting. The fields in our sample all have a *similar* distribution of thresholds, though they differ in detail. Thus each

³ After completion of the analysis it was found that field 9 did not have an on-axis target, and that the two target sources (compact open cluster Westerlund 2, and Wolf–Rayet star Wack 2134, at off-axis angles of 7.8 and 8.0 arcmin) had been erroneously included in the survey. The effect of correcting for these two sources would be a small (< 1 per cent) reduction in survey area and the removal of two sources from the bright (≥ 0.03 count s⁻¹) end of the number–flux relation. This would not change the results of the survey in any significant way.

⁴ PSS is part of the UK Starlink ASTERIX X-ray data analysis package (Allan 1992).

source will have its own associated coverage fraction within the survey, i.e. the fraction of the survey area within which it could be detected. Fig. 2 (top) shows the hard-band coverage curve for the survey. Good coverage is achieved down to ≈ 0.002 count s⁻¹, with ≈ 90 per cent of the survey area being above this threshold. Below this count rate there is a sharp drop to ≈ 20 per cent coverage at ≈ 0.001 count s⁻¹. Fig. 2 (bottom) shows the soft-band coverage curve.

Using the coverage curve it is straightforward to calculate the corrected number–flux (log N –log S) relation. For a source i , the fraction f_i of the survey area within which the source could have been detected was computed. That source then contributes $1/f_i$ to the number–flux relation, which can be found by summing over the $1/f_i$ values, as shown in Fig. 3.

3.1 Parametrization of the number–flux relation

The coverage-corrected, number–flux relation, for source count rate $S > 0.002$ count s⁻¹, was fitted with a power law $N(> S) = N_0 S^{-\alpha}$, after first subtracting an ‘extragalactic’ component. The ‘ χ^2 ’ fit was performed on the differential, binned form of the distribution, following the prescription of Lampton, Margon & Bowyer (1976) to compute the confidence ranges.

The best-fitting parameter values and one-parameter 90 per cent confidence intervals were $\alpha = 1.5$ (1.1–2.2) and $N_0 = 20$ (13–25) sources per square degree above $S > 0.002$ count s⁻¹. The joint normalization–index confidence regions are shown in Fig. 4. The extragalactic contribution was estimated from published PSPC high-latitude source counts (Hasinger et al. 1993; Branduardi-Raymont et al. 1994 – both gave similar results) suitably attenuated by Galactic absorption ($N_H \sim 5 \times 10^{21}$ cm⁻², Stark et al. 1992), as explained in Section 3.2. The estimated extragalactic contribution to the total Galactic-plane source counts is a relatively minor one; assuming zero contribution increases the normalization to $N_0 = 25$ (18–32) and has little effect on the (already rather poorly constrained) power-law index.

3.2 Contribution of extragalactic sources

The modification of the extragalactic number–flux relation by absorption in our own Galaxy was computed as follows. A ‘Galactic transmission factor’ (F_{tg}) was defined as $F_{\text{tg}} = C_a/C_u$, where C_a is the count rate from an extragalactic source after absorption by the interstellar medium (ISM) of our own Galaxy, and C_u is the count rate for zero Galactic absorption. By considering a power-law spectrum with typical energy-index values (1–2) and $N_H \approx 5 \times 10^{21}$ – 10^{22} cm⁻² (cf. Table 1), the hard-band F_{tg} was found to lie in the range ≈ 0.2 – 0.3 . The nominal value was taken as 0.3; however, the analysis was also conducted using 0.2 and 0.0, the latter corresponding to zero extragalactic source contribution. If the (unattenuated) extragalactic number–flux relation is $N_{\text{ex}}(> S)$ sources per square degree at count rate S , then, as viewed through the Galaxy, the number of extragalactic sources per square degree at count rate S' will be $N'_{\text{ex}} = N_{\text{ex}}(> S'/F_{\text{tg}})$.

4 SEARCHING FOR OPTICAL COUNTERPARTS

We have searched for optical counterparts to our X-ray sources on the basis of positional coincidence and photometric properties alone (as in Briggs et al. 2000). We used four on-line all-sky databases in the following order. First, SIMBAD was searched to

Table 2. Sources detected in the hard band (0.4–2 keV) using the PSS source searching algorithm. Columns show source number, field in which source is detected, equatorial and Galactic coordinates (J2000), significance of detection in equivalent Gaussian σ , count rate and count-rate error (count ks⁻¹) and notes. Of the 93 sources detected, four were not found in the hard band. Shown in this table is the upper limit on the count rate in the hard band for these sources. A letter ‘S’ in the notes column indicates that a source was detected in the soft band (0.1–0.4 keV) only, whilst a ‘T’ means that the source was detected in the total band (0.1–2 keV) only.

RO	F	RA	Dec.	l	b	Signif.	$C_X \pm \sigma_{C_X}$	Notes	
		(J2000)	(J2000)	(deg)		σ	(ct ks ⁻¹)		
01	1	05 44 40.27	+28 57 35.3	179.871	-0.164	4.91	2.0	0.7	
02	1	05 44 41.22	+28 47 41.3	180.014	-0.247	5.06	2.8	0.9	
03	1	05 44 41.37	+29 07 37.2	179.731	-0.073	7.00	3.8	1.0	
04	1	05 44 45.69	+28 55 06.3	179.917	-0.169	6.11	2.3	0.7	
05	1	05 44 57.62	+28 58 40.4	179.889	-0.101	12.18	5.3	0.1	
06	1	05 45 07.19	+29 09 31.5	179.753	0.023	99%	<0.8		S
07	1	05 45 13.11	+28 43 33.5	180.133	-0.184	7.83	4.5	0.1	
08	1	05 45 22.97	+29 10 59.5	179.762	0.084	13.56	8.9	0.1	
09	1	05 45 27.27	+28 57 46.7	179.958	-0.016	5.29	1.6	0.6	
10	1	05 45 56.84	+29 07 56.7	179.869	0.163	7.16	3.7	0.9	
11	2	06 14 23.50	+17 44 29.5	192.988	0.144	4.75	1.7	0.6	
12	2	06 14 35.95	+17 49 10.0	192.943	0.225	6.32	1.4	0.5	
13	2	06 14 41.85	+17 34 09.5	193.174	0.126	10.12	4.9	1.0	
14	2	06 14 42.27	+17 43 32.2	193.037	0.202	7.28	2.1	0.6	
15	2	06 14 46.78	+17 36 48.3	193.144	0.164	5.22	1.5	0.5	
16	2	06 15 17.57	+17 39 29.4	193.163	0.293	5.24	1.5	0.5	
17	2	06 15 34.03	+17 37 55.2	193.218	0.338	5.01	1.1	0.4	
18	2	06 15 43.23	+17 53 44.3	193.003	0.496	5.88	1.9	0.6	
19	2	06 15 47.51	+17 52 34.1	193.028	0.501	4.84	1.2	0.5	
20	2	06 15 54.51	+17 34 59.6	193.299	0.386	6.08	2.2	0.7	
21	2	06 16 05.30	+17 37 27.6	193.284	0.444	9.78	4.2	0.9	
22	2	06 16 24.75	+17 39 57.4	193.284	0.532	99%	<1.4		S
23	3	06 41 29.91	+04 19 56.9	207.944	-0.231	5.03	3.6	1.0	T
24	3	06 41 36.16	+04 28 55.4	207.822	-0.139	11.60	6.8	1.1	
25	3	06 41 36.24	+04 31 41.9	207.781	-0.117	7.14	3.3	0.8	
26	3	06 41 50.69	+04 20 08.5	207.980	-0.152	13.52	5.6	0.9	
27	3	06 41 59.31	+04 28 47.9	207.868	-0.054	8.99	3.2	0.7	
28	3	06 42 13.47	+04 09 31.9	208.181	-0.149	4.68	1.8	0.6	
29	3	06 42 45.14	+04 23 21.8	208.036	0.073	8.36	2.7	0.7	
30	3	06 42 45.30	+04 18 40.2	208.106	0.038	10.22	3.6	0.8	
31	3	06 43 00.59	+04 25 16.7	208.037	0.145	5.01	1.3	0.5	
32	3	06 43 11.50	+04 12 42.1	208.244	0.089	7.58	3.5	0.8	
33	4	07 01 21.23	-05 26 42.4	218.906	-0.283	7.34	4.5	1.0	
34	4	07 01 22.42	-05 24 51.6	218.881	-0.264	11.29	7.0	1.2	
35	4	07 01 25.01	-05 22 22.0	218.849	-0.236	6.08	2.9	0.8	
36	4	07 01 52.48	-05 25 51.0	218.953	-0.161	33.55	23.2	2.0	
37	4	07 01 58.50	-05 36 18.7	219.119	-0.219	14.68	10.6	1.5	
38	4	07 02 05.87	-05 33 22.5	219.090	-0.169	6.14	2.1	0.7	
39	4	07 02 30.16	-05 10 40.5	218.799	0.093	6.10	2.5	0.8	
40	4	07 02 51.91	-05 14 16.5	218.894	0.145	13.61	6.7	1.1	
41	4	07 03 07.17	-05 35 19.7	219.235	0.041	12.55	8.2	1.3	
42	4	07 03 24.52	-05 27 29.2	219.152	0.165	5.29	2.5	0.8	
43	5	07 17 30.72	-13 05 23.1	227.527	-0.278	6.96	2.3	0.5	
44	5	07 17 32.64	-13 20 28.0	227.752	-0.388	7.46	2.6	0.5	
45	5	07 17 34.27	-13 17 47.2	227.716	-0.362	5.04	1.4	0.4	
46	5	07 17 41.39	-13 22 06.3	227.793	-0.370	5.56	1.8	0.5	
47	5	07 17 43.24	-13 25 23.3	227.846	-0.389	99%	<0.5		S
48	5	07 17 49.17	-13 15 14.4	227.707	-0.288	8.91	1.8	0.4	
49	5	07 18 05.63	-12 58 28.3	227.491	-0.099	5.97	1.8	0.5	
50	5	07 18 06.08	-13 18 37.5	227.789	-0.254	6.48	1.3	0.4	
51	5	07 18 08.13	-13 19 58.1	227.812	-0.257	4.76	1.0	0.3	
52	5	07 18 10.83	-13 22 38.5	227.857	-0.268	8.37	1.9	0.4	
53	5	07 18 12.13	-13 06 34.4	227.623	-0.138	5.31	1.0	0.3	
54	5	07 18 13.02	-13 27 04.1	227.926	-0.295	6.42	2.2	0.5	

Table 2 – continued

RO	F	RA (J2000)	Dec.	l (deg)	b	Signif. σ	$C_x \pm \sigma_{C_x}$ (ct ks ⁻¹)	Notes
55	5	07 18 13.29	−13 23 54.8	227.880	−0.269	23.13	8.5	0.8
56	5	07 18 38.49	−13 01 15.7	227.594	−0.002	6.98	2.1	0.5
57	5	07 18 44.34	−13 06 47.5	227.687	−0.025	8.84	2.3	0.5
58	5	07 18 48.47	−12 57 23.4	227.556	0.063	6.06	1.9	0.5
59	5	07 19 10.30	−13 14 56.1	227.856	0.004	14.55	3.7	0.5
60	6	07 22 25.08	−15 10 59.3	229.933	−0.210	5.61	2.5	0.8
61	6	07 22 29.87	−15 04 04.6	229.841	−0.138	7.16	3.7	0.9
62	6	07 23 05.23	−15 17 46.1	230.109	−0.121	9.07	2.7	0.7
63	6	07 23 07.04	−14 58 41.3	229.832	0.035	5.31	1.7	0.6
64	6	07 23 14.56	−14 52 51.2	229.761	0.107	6.05	2.7	0.8
65	6	07 23 31.02	−15 12 20.6	230.078	0.012	9.20	3.4	0.8
66	6	07 23 33.20	−15 10 29.9	230.055	0.035	4.73	1.2	0.5
67	7	07 23 40.72	−16 08 09.3	230.916	−0.392	6.85	3.6	0.9
68	7	07 24 01.68	−16 11 40.7	231.008	−0.346	5.19	1.4	0.5
69	6	07 24 02.69	−15 05 24.8	230.037	0.179	7.54	2.6	0.7
70	6	07 24 03.44	−14 57 16.1	229.919	0.246	4.70	2.0	0.7
71	6	07 24 08.21	−14 59 29.6	229.960	0.245	5.31	2.3	0.7
72	7	07 25 18.36	−16 10 35.1	231.137	−0.067	13.80	7.0	1.1
73	7	07 25 21.41	−15 56 36.0	230.938	0.053	7.49	4.8	1.0
74	8	08 09 24.01	−33 30 00.7	251.108	−0.232	5.92	5.4	1.7
75	8	08 09 26.33	−33 20 15.2	250.976	−0.137	5.32	3.6	1.3
76	8	08 09 26.95	−33 25 16.6	251.048	−0.180	6.34	4.7	1.5
77	8	08 10 18.42	−33 06 10.3	250.879	0.143	4.99	2.4	1.0
78	9	10 22 59.46	−57 42 41.6	284.128	−0.363	6.26	4.1	1.0
79	9	10 23 38.83	−57 58 00.1	284.339	−0.532	5.33	3.1	0.9
80	9	10 23 43.65	−57 38 33.8	284.175	−0.252	6.40	3.4	0.9
81	9	10 23 50.65	−57 57 44.3	284.359	−0.514	5.44	2.8	0.8
82	9	10 23 59.78	−57 45 34.8	284.268	−0.332	27.62	33.7	2.6
83	9	10 24 14.97	−57 39 46.8	284.245	−0.232	5.43	1.9	0.6
84	9	10 24 47.19	−57 32 54.8	284.245	−0.097	4.80	2.1	0.7
85	9	10 25 01.52	−57 54 24.9	284.462	−0.384	4.92	2.0	0.7
86	9	10 25 35.09	−57 50 50.8	284.493	−0.294	9.77	3.2	0.7
87	9	10 25 45.58	−57 35 30.9	284.378	−0.065	10.28	6.7	1.2
88	9	10 25 52.33	−57 54 00.0	284.554	0.318	5.97	2.3	0.7
89	9	10 25 54.37	−57 37 57.4	284.416	−0.089	8.54	3.6	0.8
90	9	10 25 55.13	−57 48 52.3	284.514	−0.243	68.29	95.5	3.9
91	9	10 26 03.40	−57 59 15.5	284.621	−0.380	27.26	29.3	2.4
92	9	10 26 04.09	−57 46 38.6	284.511	−0.201	5.34	2.2	0.7
93	9	10 26 11.14	−57 56 55.8	284.615	−0.338	12.58	8.7	1.3

find potential counterparts over a wide range of wavelengths. Secondly, we searched the Tycho-2 catalogue (Høg et al. 2000) for bright ($V \leq 12$) stellar counterparts. Thirdly, the USNO-A2.0 (Monet et al. 1998) catalogue was searched for all possible optical counterparts detected above the Palomar/ESO/SRC plate limit ($V \leq 19$). Finally, we searched the 2MASS Second Incremental Data Release (Cutri et al. 2000) for near-infrared counterparts. The 2MASS photometry is more reliable than that found in the USNO-A2.0 and its three bands allow two-colour diagrams to constrain better the class of the object. All potential counterparts are listed in Table 4.

4.1 SIMBAD

We employed a uniform search radius of 35 arcsec around each X-ray source position. In our fields we would expect this search region to yield four SIMBAD objects by chance. We find SIMBAD counterparts to 29 of our sources. Eleven matches are simply with

X-ray sources detected in previous surveys, or in the field 9 observation already presented by Belloni & Mereghetti (1994, hereafter BM94). No source was matched with more than one non-X-ray SIMBAD object. BM94 associated two sources with Wolf-Rayet stars and one with an O7 star. Source 11 was associated with a compact H II region.⁵ Other stars accounted for 13 matches, in

⁵ IRAS 06114 + 1745 : classed as an ‘ultracompact H II region’ by Bronfman, Nyman & May (1996); detected as a water maser and considered to be a star-forming region by Palagi et al. (1993); and noted as ‘nebulous’ and associated with ‘a B-type star that suffers appreciable circumstellar extinction’ by Cohen, Jones & Walker (1989). It appears extended in optical and near-IR images [and is proposed as a galaxy by Seeberger, Saurer & Weinberger (1996) on the basis of this extension], although it is not flagged as such in 2MASS; instead 12 point sources are detected in the region. These have peculiar, mostly heavily reddened, near-IR colours and may be spurious or heavily absorbed stars within the cloud. Several H II regions are known to be associated with diffuse X-ray emission produced by hot plasma (e.g. Carina nebula, $L_X \sim 10^{35}$ erg s⁻¹).

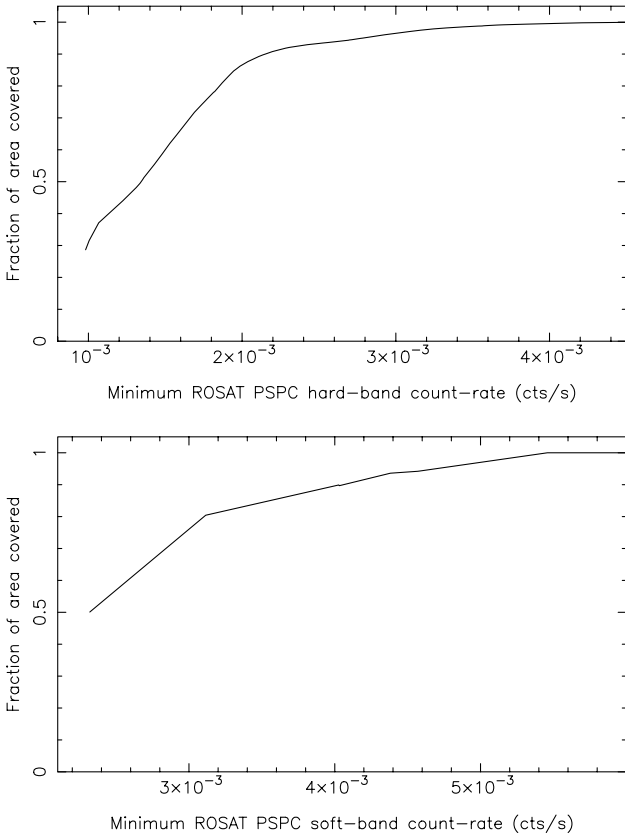


Figure 2. The coverage curves for the survey in the hard (top) and soft (bottom) bands. These take into account the differences in area between fields. Good coverage is achieved down to $\approx 0.002 \text{ count s}^{-1}$ in the hard band with around 90 per cent of the survey being above this count rate.

addition to two radio sources. All matches were found within 20 arcsec except for the brightest counterpart, a 6th magnitude K-type giant 31 arcsec from source 81.

4.2 Tycho-2

Tycho-2 (Høg et al. 2000) is a catalogue of the 2.5 million brightest stars in the sky. It contains astrometric, proper motion

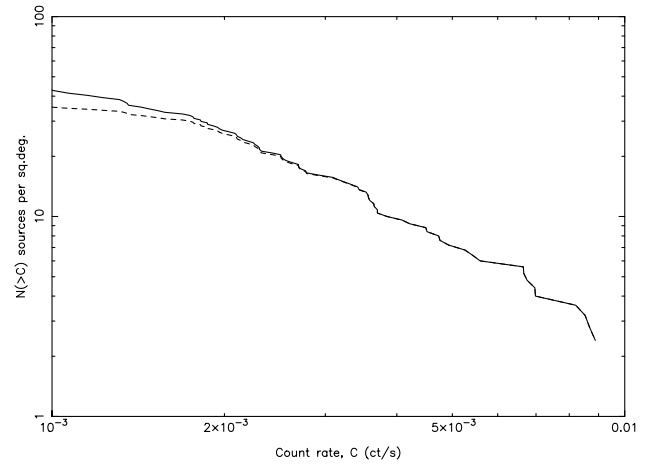


Figure 3. The hard-band (0.4–2.0 keV) number–flux relation, here shown in integral format, derived from the 89 hard-band sources detected in our nine PSPC fields. The dotted line shows the raw counts and the solid line shows the coverage-corrected $\log N$ – $\log S$.

and two-band photometric information based on data taken by the star-mapper on the ESA *Hipparcos* satellite. The catalogue’s 90 per cent completeness level is at $V \sim 11.5$. The Tycho-2 search yielded all 13 stellar matches made in SIMBAD, and six further stellar candidates, with no ambiguous cases. Excepting the K-type giant, and a 12th magnitude star 32 arcsec from source 55, all matches were made within 20 arcsec of the X-ray source position. We converted the Tycho raw V_T and B_T band magnitudes to approximate Johnson photometry using the transformations: $V = V_T + 0.09(B_T - V_T)$ and $(B - V) = 0.85(B_T - V_T)$ (ESA 1997).

4.3 USNO-A2.0

USNO-A2.0 (Monet et al. 1998) is a catalogue of over 500 million objects, containing astrometric data and the blue and red magnitudes for each, based on a re-reduction of the Precision Measuring Machine (PMM) scans of the POSS-I, SRC and ESO plates. The faintest objects in our region of interest are of 19th magnitude, and the catalogue is reportedly complete to $R \sim 18$, with the proviso that the source is detected on both blue and red

Table 3. Sources detected in the soft band (0.1–0.4 keV) using the PSS source searching algorithm. Columns show the source number, field in which the source was found, coordinates, significance of detection, count rate and count-rate error (count ks^{-1}) and hardness ratio. Hardness ratio (HR) is defined as $(H - S)/(H + S)$ where H is the hard-band count rate and S is the count rate in the soft band.

RO	F	RA	Dec.	l	b	Signif.	$C_X \pm \sigma_{C_X}$			HR $\pm \sigma_{HR}$	
		(J2000)		(deg)		σ	(ct ks $^{-1}$)				
06	1	05 45 07.19	+29 09 31.5	179.75318	0.02296	5.15	4.6	1.2	< -0.64		
16	2	06 15 17.57	+17 39 29.4	193.16395	0.29364	8.17	4.6	0.9	-0.51	0.14	
21	2	06 16 05.30	+17 37 27.6	193.28400	0.44415	4.84	3.1	0.9	0.15 0.18		
22	2	06 16 24.75	+17 39 57.4	193.28414	0.53188	6.26	5.5	1.2	< -0.69		
24	3	06 41 36.16	+04 28 55.4	207.82292	-0.13909	8.74	7.1	1.2	-0.02	0.12	
25	3	06 41 36.24	+04 31 41.9	207.78194	-0.11763	4.99	4.0	1.1	-0.10	0.18	
36	4	07 01 52.48	-05 25 51.0	218.95326	-0.16154	19.75	6.1	1.2	0.58 0.07		
47	5	07 17 43.24	-13 25 23.3	227.84553	-0.38908	5.08	2.3	0.6	< -0.40		
67	7	07 23 40.72	-16 08 09.3	230.91691	-0.39249	7.62	5.8	1.2	-0.24	0.15	
78	9	10 22 59.46	-57 42 41.6	284.12897	-0.36381	5.77	4.0	1.0	0.01 0.17		
91	9	10 26 03.40	-57 59 15.5	284.62120	-0.38046	7.42	4.4	1.0	0.74 0.05		
93	9	10 26 11.14	-57 56 55.8	284.61527	-0.33847	9.75	7.3	1.3	0.09 0.12		

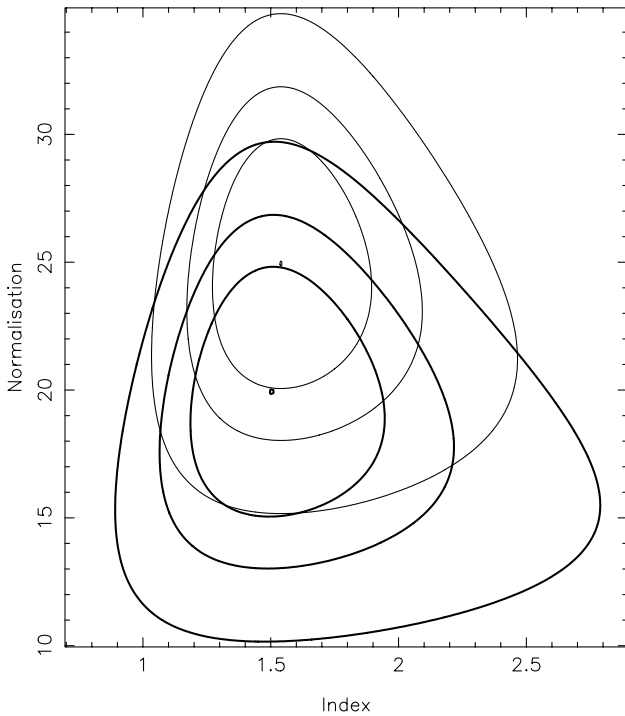


Figure 4. The two-parameter, normalization and index, power-law fit to $\log N - \log S$. The extragalactic contribution has been subtracted, having been estimated using the high-latitude source counts from Hasinger et al. (1993) and allowing for transmission factors of 0.3 (lower, thicker contours) and zero (upper, thinner contours). Regions of 68, 90 and 99 per cent confidence are shown.

plates. The PMM has problems in crowded fields, missing some obvious sources and detecting spurious sources. Excepting fields 5 and 9, the USNO seems unproblematic except for the odd obvious missed source and spurious detection (of order 1–10 per field). The centre of field 5 is dominated by the H II region NGC 2359, although none of our X-ray sources are in this area, while the west side of field 9 (closest to the Galactic Centre, and hence most densely populated) has considerable holes in its USNO coverage due to the H II region Gum 29 and the compact open clusters NGC 3247 and Westerlund 2, the latter housing one of our X-ray sources.

To keep the number of matches to a reasonable level, we reduced our search radius to 20 arcsec. Previous experience with PSPC observations in the Hyades (Morley 1998) and the above SIMBAD and Tycho-2 searches indicate that we would expect to miss ≤ 5 per cent of counterparts. We found at least one USNO-A2.0 match for all but seven of our 93 sources, although these seven include source 81, with its bright counterpart 31 arcsec away, and source 82, which sits in a very confused region of stars in the heart of the open cluster Westerlund 2. We re-searched the catalogue using a search radius of 35 arcsec for these five unmatched objects and found matches for three of them, leaving only sources 19 and 73 without potential optical counterparts.

The number of matched objects per source varied from zero to seven, and was field-dependent. The number of objects expected to fall into our search area by chance varied from < 1 in field 2 to > 4 in field 9, chiefly because the star density increases along the plane from the anticentre direction (fields 1 and 2), although if we consider only $R < 16$ this drops to < 1 even in field

9. In general, we expect multiple potential counterparts to each X-ray source.

4.4 2MASS

The Two Micron All Sky Survey (2MASS) (Cutri et al. 2000) is uniformly scanning the entire sky in three near-infrared bands [J (1.25 μm), H (1.65 μm) and K_S (2.17 μm)] for point sources brighter than about 1 mJy in each band. The Second Incremental Data Release covers ~ 47 per cent of the sky, including seven of our fields (fields 3 and 9 are not included), but has holes close to bright red stars (e.g. in field 2). This catalogue contains astrometric information and photometric magnitudes in the three bands, and a cross-correlation with objects in the USNO-A, making it ideal for following up the USNO search.

Using a 20 arcsec search radius, 185 matches were found, of which 42 were not coincident (within 5 arcsec) with USNO objects, including three faint potential counterparts to source 19, thus leaving source 73 as the only source with no potential optical counterpart.

5 CLASSIFICATION OF OPTICAL COUNTERPARTS

We have found more than one potential optical counterpart for most of our X-ray sources. We have treated each candidate as the real counterpart and classified it on the basis of its X-ray, optical and near-infrared photometry, and then made a judgement on the best classification for the source. Our classification procedure was as follows.

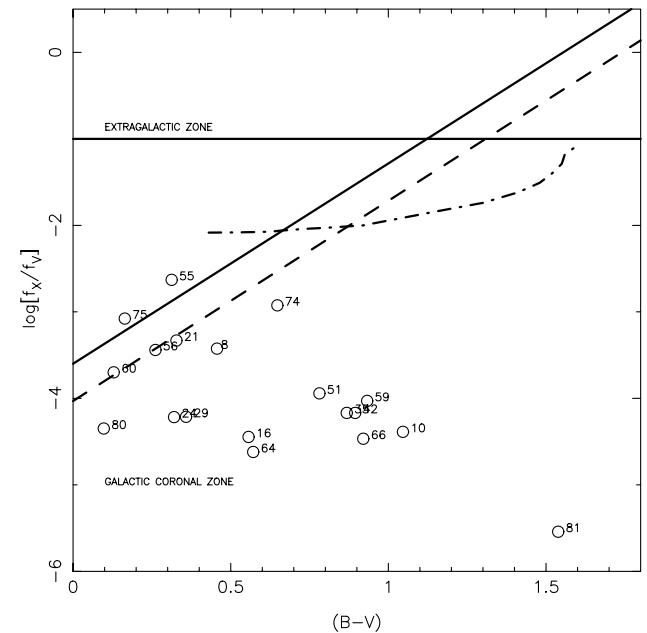


Figure 5. Plot of $\log(f_X/f_V)$ versus $B - V$ for all potential optical counterparts found in the Tycho-2 catalogue. The plotted quantities are not corrected for reddening or absorption. Numbers refer to the associated X-ray source. The bold diagonal solid and dashed lines are expected to bound zones of the diagram containing, respectively, 98 and 90 per cent of coronal sources (derived from fig. 7 in Stocke et al. 1991). The bold horizontal line marks the value above which extragalactic sources are expected to dominate. The bold dot-dashed line indicates the saturation threshold of $\log(L_X/L_{\text{bol}}) = -3$ for main-sequence stars.

Table 4. Possible optical and near-infrared counterparts to X-ray sources detected in this survey. The catalogues and search radii used are described in the text. The columns show: designation (comprising source number from Table 2 and a letter running in alphabetical order with separation from X-ray source position); position (J2000; from USNO/Tycho-2, SIMBAD or 2MASS, as indicated by column 5); separation from X-ray source position in arcsec; source of position and optical photometry (U = USNO-A2.0; T = Tycho-2; S = SIMBAD; 2 = 2MASS); optical magnitude (V if photometry is from Tycho-2; R from USNO-A2.0); optical colour ($B - V$ if photometry is from Tycho-2; $B - R$ from USNO-A2.0); $\log(f_X/f_{\text{opt}})$ ($\log(f_X/f_V)$ if photometry is from Tycho-2; $\log(f_X/f_R)$ from USNO-A2.0); classification from $\log(f_X/f_{\text{opt}})$ versus colour diagram (see Figs 5 and 6); J magnitude, $J - H$ and error; $H - K_S$ and error; flag indicating whether the position on a near-IR two-colour diagram is consistent with an MS star; spectral type [estimated from near-IR photometry using the MS colours table of Bessell & Brett (1988), unless the luminosity class is given, whereby the spectral type is taken from SIMBAD]; and further notes on the object (see text for details on distance and luminosity determination; luminosity units are erg s^{-1}).

Des.	RA	Dec.	Sep.	Ref.	m_{opt}	Col.	$[f_X/f_{\text{opt}}]$	Cl.	J	$(J - H)$	$(H - K_S)$	MS	Sp.	Notes	
1	A	05 44 39.70	+28 57 20.2	16.9	U	18.3	1.2	-0.43	E	16.01	0.46 ± 0.16	0.31 ± 0.21	Y	?	
2	A	05 44 40.88	+28 47 24.1	17.8	U	17.6	1.8	-0.57	E	15.60	0.59 ± 0.13	0.17 ± 0.15	Y	?	
3	A	05 44 40.46	+29 07 24.2	17.7	U	14.2	2.4	-1.79	C	12.01	0.62 ± 0.05	0.20 ± 0.04	Y	KM	
4	A	05 44 47.62	+28 55 15.6	27.0	U	17.8	1.4	-0.51	E	15.82	0.68 ± 0.13	0.04 ± 0.17	Y	KM?	
5	A	05 44 57.30	+28 58 35.1	6.7	2			>0.27		16.03	0.65 ± 0.16	0.58 ± 0.18	Y	?	
5	B	05 44 56.31	+28 58 32.3	19.0	2			>0.27		16.48	>0.21	<0.87	N		
6	A	05 45 06.04	+29 09 31.9	15.1	U	17.5	1.3	-1.24	N	15.68	0.44 ± 0.13	-0.17 ± 0.22	Y	?	
7	A	05 45 12.86	+28 43 37.1	4.8	U	16.6	1.5	-0.76	E	15.22	0.43 ± 0.09	0.08 ± 0.13	Y	GK	
7	B	05 45 13.36	+28 43 21.0	12.9	U	17.9	1.3	-0.24	E	15.94	0.85 ± 0.12	0.33 ± 0.15	Y	KM?	
7	C	05 45 12.08	+28 43 19.0	19.8	2			>0.20		16.62	>0.65		?		
8	A	05 45 22.60	+29 10 57.1	5.5	T	10.4	0.5	-3.42	C	9.50	0.28 ± 0.04	0.02 ± 0.04	Y	F8	$d \sim 190$ pc, $\log(L_X) \sim 29.6$
8	B	05 45 23.55	+29 10 57.6	7.8	U	17.2	0.7	-0.22	E						Spurious
8	C	05 45 21.93	+29 10 53.9	14.7	U	14.7	1.8	-1.22	C	14.52	0.49 ± 0.07	0.14 ± 0.07	Y	K	
8	D	05 45 22.61	+29 10 44.9	15.4	U	16.5	2.1	-0.50	E						Spurious
9	A	05 45 27.60	+28 57 53.0	7.6	U	15.5	2.6	-1.65	C	12.66	0.84 ± 0.04	0.25 ± 0.04	Y	M?	
9	B	05 45 25.99	+28 57 41.7	17.5	U	13.0	1.1	-2.65	C	11.90	0.44 ± 0.04	0.13 ± 0.04	Y	GK	
9	C	05 45 25.84	+28 57 57.2	21.5	U	15.0	0.9	-1.85	N	15.95	0.54 ± 0.14	0.54 ± 0.16	Y		
10	A	05 45 57.17	+29 07 46.0	11.5	U	13.7	3.3	-2.01	C						Spurious
10	B	05 45 56.23	+29 08 07.2	13.2	U	14.5	1.9	-1.69	C						
10	C	05 45 56.17	+29 07 46.4	13.8	T	8.9	1.0	-4.39	C	6.80	0.52 ± 0.02	0.18 ± 0.02	Y	K0V	HD 247187, $d \sim 40$ pc, $\log(L_X) \sim 27.8$
10	D	05 45 55.41	+29 07 49.9	19.9	U	13.2	3.4	-2.21	C						Spurious
11	A	06 14 23.52	+17 44 32.8	3.3	2			>-0.22		>13.92	<1.18	-0.03 ± 0.08	?		
11	B	06 14 23.85	+17 44 30.3	5.0	2			>-0.22		>14.71	<0.10	0.81 ± 0.14	?		
11	C	06 14 22.88	+17 44 32.3	9.3	U	13.8	3.2	-2.30	C	14.93	1.75 ± 0.08	0.51 ± 0.05	N		
11	D	06 14 23.41	+17 44 39.0	9.6	U	9.9	3.3	-3.86	C	11.19	0.71 ± 0.05	0.45 ± 0.04	Y		IRAS 06114+1745, H II region
11	E	06 14 22.94	+17 44 22.6	10.6	2			>-0.22		16.68	1.41 ± 0.23	0.72 ± 0.16	N		
11	F	06 14 24.24	+17 44 26.8	10.9	2			>-0.22		>15.68	<0.22	0.82 ± 0.22	?		
11	G	06 14 24.17	+17 44 37.6	12.5	2			>-0.22		15.33	1.13 ± 0.14	0.71 ± 0.11	N		
11	H	06 14 23.20	+17 44 43.0	14.2	2			>-0.22		14.64	1.19 ± 0.13	0.75 ± 0.09	N		
11	I	06 14 23.56	+17 44 13.3	16.3	2			>-0.22		15.97	1.62 ± 0.11	1.09 ± 0.07	N		
11	J	06 14 23.61	+17 44 47.4	17.9	2			>-0.22		>14.55		<-0.19	?		
11	K	06 14 22.52	+17 44 41.6	18.5	U	16.8	1.2	-1.10	N	15.22	1.52 ± 0.15	0.90 ± 0.11	N		
11	L	06 14 22.74	+17 44 45.7	19.5	2			>-0.22		16.17	1.55 ± 0.23	$2.13 \pm >-0.26$	N		
12	A	06 14 35.50	+17 49 17.5	9.8	U	14.6	0.9	-2.05	N						
12	B	06 14 34.93	+17 49 08.9	14.6	2			>-0.29		15.82	0.59 ± 0.11	0.16 ± 0.20	Y	KM	
13	A	06 14 41.65	+17 34 21.6	12.5	U	13.2	1.0	-2.08	C						
13	B	06 14 41.55	+17 33 56.5	13.7	U	13.7	2.4	-1.88	C						
14	A	06 14 42.11	+17 43 38.4	6.6	U	11.9	2.1	-2.97	C						
14	B	06 14 42.16	+17 43 15.8	16.5	U	16.8	1.9	-1.01	C						

Table 4 – continued

Des.	RA	Dec.	Sep.	Ref.	m_{opt}	Col.	$[f_X/f_{\text{opt}}]$	Cl.	J	$(J - H)$	$(H - K_S)$	MS	Sp.	Notes	
15	A	06 14 47.27	+17 36 59.7	13.3	U	18.3	1.3	-0.55	E						
16	A	06 15 16.65	+17 39 33.5	13.8	U	12.9	1.0	-2.72	C	11.83	0.24 ± 0.06	0.03 ± 0.06	Y	F	
16	B	06 15 18.13	+17 39 42.0	14.0	T	9.8	0.6	-4.45	C	8.49	0.34 ± 0.02	0.05 ± 0.04	Y	G5	GSC 01318-00940, $d \sim 90$ pc, $\log(L_X) \sim 28.2$
16	C	06 15 18.65	+17 39 38.1	17.7	2			> -0.28		14.14	0.30 ± 0.13	0.31 ± 0.13	Y		
17	A	06 15 34.62	+17 37 57.0	8.6	U	17.6	1.9	-0.98	C	15.54	0.76 ± 0.09	0.19 ± 0.13	Y	KM	
17	B	06 15 34.33	+17 37 39.5	16.3	U	16.1	1.6	-1.58	C	14.44	0.61 ± 0.05	0.12 ± 0.07	Y	K	
17	C	06 15 33.05	+17 38 04.5	16.9	U	12.6	0.5	-2.98	C	11.79	0.17 ± 0.04	0.10 ± 0.05	Y	F	
18	A	06 15 43.53	+17 53 50.3	7.4	U	13.7	1.4	-2.30	C	12.69	0.44 ± 0.04	0.04 ± 0.04	Y	GK	
18	B	06 15 43.08	+17 54 01.2	17.0	U	16.0	2.0	-1.38	C	13.63	0.75 ± 0.05	0.19 ± 0.05	Y	M?	
19	A	06 15 47.27	+17 52 43.4	9.9	2			> -0.39		16.29	0.75 ± 0.15	0.02 ± 0.23	Y	M?	
19	B	06 15 46.97	+17 52 26.9	10.5	2			> -0.39		15.39	0.75 ± 0.08	0.17 ± 0.10	Y	M?	
19	C	06 15 47.75	+17 52 46.7	13.1	2			> -0.39		15.60	0.75 ± 0.08	0.21 ± 0.11	Y	M?	
20	A	06 15 53.52	+17 34 54.6	15.0	U	18.0	1.4	-0.50	E	16.24	0.50 ± 0.16	0.29 ± 0.26	Y	GKM?	
20	B	06 15 53.75	+17 34 44.4	18.7	2			> -0.10		16.26	0.71 ± 0.14	0.40 ± 0.21	Y	M?	
21	A	06 16 05.34	+17 37 33.7	6.1	2			> 0.17		16.45	1.00 ± 0.17	0.22 ± 0.21	N		
21	B	06 16 04.30	+17 37 31.7	14.9	U	17.9	1.3	-0.27	E						
21	C	06 16 06.12	+17 37 16.6	16.1	2			> 0.17		16.84	1.07 ± 0.23	> 0.20	?		
21	D	06 16 04.89	+17 37 46.0	19.4	T	11.4	0.3	-3.33	C	10.32	0.31 ± 0.05	0.01 ± 0.05	Y	F8	$d \sim 300$ pc, $\log(L_X) \sim 29.7$
22	A	06 16 23.75	+17 40 13.9	21.8	U	16.1	2.6	-1.39	C	12.71	0.59 ± 0.05	0.31 ± 0.05	Y	M	
23	A	06 41 30.86	+04 19 57.1	14.3	U	15.4	0.9	-1.23	N						
23	B	06 41 30.70	+04 20 08.4	16.6	U	18.4	1.5	-0.13	E						
23	C	06 41 30.95	+04 20 05.0	17.5	U	15.5	2.2	-1.29	C						
23	D	06 41 31.03	+04 20 02.4	17.7	U	16.6	1.3	-0.85	N						
24	A	06 41 36.07	+04 28 53.0	3.8	T	8.7	0.3	-4.22	C				F4III	HD 48031, $d \sim 250$ pc, $\log(L_X) \sim 29.7$	
25	A	06 41 35.71	+04 31 50.5	11.7	U	12.4	0.4	-2.57	N						
25	B	06 41 36.04	+04 31 27.8	14.5	U	18.7	0.9	-0.05	E						
26	A	06 41 50.79	+04 20 09.0	1.5	U	15.7	0.6	-1.02	N						
26	B	06 41 50.9	+04 20 10	3.5	S			> 0.30						Radio, [SCR92] 207.98-0.15	
26	C	06 41 49.66	+04 20 09.5	15.4	U	17.1	2.8	-0.46	C						
27	A	06 41 59.13	+04 28 47.2	2.7	U	15.0	1.9	-1.55	C						
27	B	06 41 58.90	+04 28 29.2	19.7	U	17.4	1.8	-0.59	E						
28	A	06 42 13.04	+04 09 26.4	8.4	U	16.7	1.8	-1.12	C						
28	B	06 42 13.66	+04 09 22.7	9.7	U	15.6	0.4	-1.56	N						
29	A	06 42 45.26	+04 23 29.1	7.0	T	9.7	0.4	-4.21	N					GSC 00155-03305	
29	B	06 42 45.74	+04 23 15.0	11.2	U	13.8	2.6	-2.10	C						
30	A	06 42 44.45	+04 18 50.2	16.1	U	18.6	1.0	-0.06	E						
31	A	06 43 00.15	+04 25 15.7	6.6	U	12.7	1.4	-2.85	C						
31	B	06 43 11.37	+04 12 57.1	16.6	U	16.6	1.0	-1.29	N						
32	A	06 43 11.20	+04 12 45.9	5.8	U	13.7	0.9	-2.02	N						
32	B	06 43 11.37	+04 12 57.1	15.1	U	18.6	1.0	-0.06	E						
33	A	07 01 20.93	-05 26 54.0	12.4	U	12.7	1.5	-2.32	C	11.86	0.42 ± 0.03	0.10 ± 0.03	Y	GK	

Table 4 – *continued*

Des.	RA	Dec.	Sep.	Ref.	m_{opt}	Col.	$[f_X/f_{\text{opt}}]$	Cl.	J	$(J - H)$	$(H - K_S)$	MS	Sp.	Notes
34	A	07 01 23.02	-05 24 52.3	8.9	U	16.7	0.4	-0.53	E	15.07	0.31 ± 0.07	0.26 ± 0.10	Y	
34	B	07 01 22.66	-05 24 39.8	12.3	2			>0.39		14.50	0.37 ± 0.05	0.08 ± 0.08	Y	
34	C	07 01 21.52	-05 24 53.6	13.6	2			>0.39		16.26	>2.22		?	
34	D	07 01 21.43	-05 24 57.1	15.8	U	14.3	1.2	-1.49	N	12.59	0.61 ± 0.03	0.07 ± 0.04	Y	
34	E	07 01 22.54	-05 24 34.1	17.6	U	12.2	1.3	-2.33	C	12.19	0.29 ± 0.04	0.06 ± 0.04	Y	FG
34	F	07 01 22.17	-05 24 32.9	19.1	U	15.3	1.4	-1.09	N	15.34	0.49 ± 0.09	0.17 ± 0.14	Y	
35	A	07 01 26.11	-05 22 26.0	17.0	U	16.3	1.5	-1.06	N	15.94	0.75 ± 0.12	0.07 ± 0.18	Y	
35	B	07 01 24.76	-05 22 39.0	16.6	T	9.7	0.9	-4.17	C	8.12	0.46 ± 0.04	0.14 ± 0.04	Y	K1
36	A	07 01 52.30	-05 25 57.9	7.4	U	11.9	1.0	-1.92	N	10.59	0.43 ± 0.03	0.12 ± 0.03	Y	GK
36	B	07 01 51.38	-05 26 01.5	19.5	U	17.9	0.5	0.48	E	16.43	0.74 ± 0.18	0.30 ± 0.24	Y	KM?
37	A	07 01 58.32	-05 36 19.8	2.9	U	17.4	1.7	-0.07	E					
37	B	07 01 58.93	-05 36 33.0	15.7	U	17.6	0.4	0.01	E					
38	A	07 02 05.04	-05 33 20.8	12.5	U	16.3	1.1	-1.21	N	14.66	0.66 ± 0.05	0.10 ± 0.07	Y	KM
38	B	07 02 05.21	-05 33 34.5	15.5	2			>-0.13		16.50	0.54 ± 0.21	>-0.13	N	
38	C	07 02 06.40	-05 33 38.3	17.7	U	17.9	1.0	-0.57	E	16.70	0.73 ± 0.23	>0.39	?	
38	D	07 02 05.70	-05 33 03.0	19.6	U	17.9	0.8	-0.57	E	15.81	0.74 ± 0.10	0.16 ± 0.15	Y	KM?
39	A	07 02 31.00	-05 10 50.4	16.0	U	16.0	1.0	-1.25	N	16.01	0.12 ± 0.34	0.77 ± 0.38	N	
39	B	07 02 31.24	-05 10 35.2	17.0	U	18.0	1.0	-0.45	E	16.16	0.52 ± 0.15	0.20 ± 0.24	Y	
39	C	07 02 31.08	-05 10 51.8	17.8	U	15.8	0.9	-1.33	N	14.72	0.41 ± 0.06	0.16 ± 0.09	Y	GK?
40	A	07 02 51.67	-05 14 07.8	9.4	U	18.9	0.1	0.33	E	16.66	0.76 ± 0.21	1.26 ± 0.19	N	
40	B	07 02 52.62	-05 14 21.6	11.7	U	18.0	0.4	-0.03	E	15.99	0.29 ± 0.17	0.21 ± 0.25	Y	
40	C	07 02 52.26	-05 14 27.7	12.3	U	18.8	0.1	0.29	E					
40	D	07 02 51.24	-05 14 24.8	12.9	U	17.3	1.5	-0.31	E	15.94	0.57 ± 0.13	0.12 ± 0.21	Y	KM?
40	E	07 02 52.91	-05 14 20.3	15.3	U	19.2	0.0	0.45	E					
40	F	07 02 51.14	-05 14 06.2	15.5	U	18.6	0.7	0.21	E	16.08	0.59 ± 0.14	0.29 ± 0.20	Y	KM?
41	A	07 03 07.50	-05 35 23.3	6.1	U	12.6	1.2	-2.10	C	10.81	0.60 ± 0.04	0.09 ± 0.04	Y	K
41	B	07 03 06.56	-05 35 18.4	9.2	U	17.2	1.2	-0.26	E	14.82	0.70 ± 0.06	0.17 ± 0.07	Y	
41	C	07 03 08.44	-05 35 17.3	19.2	U	17.0	1.2	-0.34	E	14.55	0.69 ± 0.05	0.18 ± 0.07	Y	
41	D	07 03 08.39	-05 35 27.9	20.0	U	17.6	0.6	-0.10	E	16.03	0.27 ± 0.17	0.31 ± 0.26	Y	
42	A	07 03 24.15	-05 27 37.1	9.6	U	16.3	1.4	-1.13	C	15.70	0.42 ± 0.23	-0.13 ± 0.30	Y	
42	B	07 03 25.16	-05 27 31.5	9.8	T	9.9	0.9	-4.17	C	7.91	0.57 ± 0.04	0.12 ± 0.05	Y	K4
42	C	07 03 23.73	-05 27 34.5	12.9	2			>-0.05		16.49	0.86 ± 0.28	0.25 ± 0.25	Y	
42	D	07 03 25.16	-05 27 38.4	13.2	2			>-0.05		12.36	>-2.23	<2.64	?	
42	E	07 03 24.64	-05 27 10.6	18.7	U	16.6	1.9	-1.01	N					
43	A	07 17 31.04	-13 05 29.0	7.6	U	17.6	0.6	-0.64	E	15.60	0.48 ± 0.09	0.01 ± 0.19	Y	GK??
43	B	07 17 29.87	-13 05 27.8	13.2	U	17.0	0.8	-0.88	N	15.48	0.49 ± 0.10	0.10 ± 0.15	Y	GK?
43	C	07 17 29.97	-13 05 14.0	14.3	2			>-0.08		16.22	0.78 ± 0.14	-0.06 ± 0.27	Y	
43	D	07 17 31.58	-13 05 38.5	19.9	U	18.3	0.4	-0.36	E	16.06	0.45 ± 0.15	>0.37		
44	A	07 17 32.75	-13 20 23.6	4.7	U	12.6	2.4	-2.60	C	13.05	0.31 ± 0.05	0.07 ± 0.05	Y	FG
44	B	07 17 32.06	-13 20 29.4	8.6	U	11.9	2.9	-2.88	C	10.06	0.86 ± 0.03	0.20 ± 0.04	Y	

GSC 04822-00365,
 $d \sim 50$ pc, $\log(L_X) \sim 28.0$
 2E 0659.4-0521

BD-05 1938,
 $d \sim 40$ pc, $\log(L_X) \sim 27.7$

Table 4 – *continued*

Des.	RA	Dec.	Sep.	Ref.	m_{opt}	Col.	$[f_X/f_{\text{opt}}]$	Cl.	J	$(J - H)$	$(H - K_S)$	MS	Sp.	Notes	
44	C	07 17 32.71	-13 20 13.6	14.4	U	14.7	0.5	-1.76	N	15.14	0.01 ± 0.16	0.31 ± 0.19	N		
44	D	07 17 32.20	-13 20 41.3	14.8	U	16.9	1.4	-0.88	N	16.03	0.38 ± 0.17	0.28 ± 0.25	Y		
44	E	07 17 32.62	-13 20 11.7	16.3	2			> -0.04		14.39	0.35 ± 0.07	0.25 ± 0.09	Y		
44	F	07 17 33.53	-13 20 17.0	17.1	U	16.1	1.8	-1.20	C	13.75	0.72 ± 0.04	0.20 ± 0.05	Y	M?	
44	G	07 17 32.00	-13 20 10.6	19.7	U	16.9	0.7	-0.88	N	15.83	0.64 ± 0.11	-0.19 ± 0.22	Y		
45	A	07 17 34.06	-13 17 37.6	10.1	U	15.4	0.8	-1.76	N	14.44	0.23 ± 0.06	0.14 ± 0.09	Y	F?	
45	B	07 17 33.46	-13 17 58.5	16.3	U	16.0	1.3	-1.52	N	14.47	0.62 ± 0.06	0.11 ± 0.07	Y	KM	
45	C	07 17 35.51	-13 17 43.1	18.6	U	15.7	0.7	-1.64	N	14.46	0.36 ± 0.07	0.13 ± 0.09	Y	G?	
46	A	07 17 41.53	-13 22 09.4	3.3	U	16.8	0.2	-1.07	N	14.86	0.37 ± 0.07	0.13 ± 0.10	Y	GK?	
46	B	07 17 42.51	-13 22 02.5	16.9	U	18.2	0.9	-0.51	E	16.31	0.65 ± 0.17	> -1.07	N		
46	C	07 17 40.22	-13 22 03.6	17.4	U	18.0	1.1	-0.59	E	16.17	0.23 ± 0.22	> 0.39	?		
47	A	07 17 42.58	-13 25 27.7	10.6	U	18.2	0.1	-1.06	N	16.31	0.48 ± 0.20	> -0.17	N		
47	B	07 17 43.79	-13 25 15.6	11.1	U	16.2	1.4	-1.86	C	13.68	0.69 ± 0.04	0.15 ± 0.05	Y	KM	
47	C	07 17 44.41	-13 25 20.2	17.3	U	14.8	0.7	-2.42	C	13.74	0.33 ± 0.04	0.06 ± 0.06	Y	FG	
47	D	07 17 43.08	-13 25 42.1	19.0	U	15.4	0.7	-2.18	C	13.95	0.34 ± 0.04	0.07 ± 0.06	Y	FG	
48	A	07 17 49.47	-13 15 23.4	10.1	U	17.9	1.4	-0.64	E	16.60	0.58 ± 0.24	0.48 ± 0.32	Y		
48	B	07 17 49.08	-13 15 25.0	10.7	U	15.8	0.5	-1.48	N	14.43	0.38 ± 0.06	0.04 ± 0.09	Y	GK	
48	C	07 17 48.01	-13 15 10.1	17.5	U	17.6	1.0	-0.76	E	16.00	0.46 ± 0.15	0.20 ± 0.26	Y		
49	A	07 18 06.27	-12 58 32.4	10.2	U	12.0	1.4	-2.99	C	11.10	0.25 ± 0.04	0.05 ± 0.04	Y	F	
49	B	07 18 04.59	-12 58 30.4	15.3	U	17.9	0.7	-0.63	E	16.07	0.46 ± 0.17	> 0.80	?		
49	C	07 18 05.42	-12 58 43.7	15.7	U	17.4	0.9	-0.83	N	15.76	0.72 ± 0.11	0.35 ± 0.15	Y		
49	D	07 18 06.67	-12 58 20.8	16.9	2			> -0.19		15.71	0.57 ± 0.12	0.20 ± 0.18	Y		
50	A	07 18 06.00	-13 18 35.6	2.3	2			> -0.32		14.31	0.65 ± 0.05	0.13 ± 0.07	Y	KM	
50	B	07 18 06.40	-13 18 35.9	5.0	2			> -0.32		11.68	0.19 ± 0.04	0.17 ± 0.04	Y	F?	
50	C	07 18 05.80	-13 18 48.5	11.7	U	17.3	0.4	-1.00	N	15.63	0.43 ± 0.12	-0.05 ± 0.20	Y		
50	D	07 18 06.91	-13 18 43.4	13.5	U	14.3	1.9	-2.20	C	12.63	0.70 ± 0.04	0.08 ± 0.04	Y	KM	
50	E	07 18 05.54	-13 18 23.2	16.3	2			> -0.32		16.04	-0.13 ± 0.35	> 1.09	?		
50	F	07 18 06.12	-13 18 20.7	16.8	U	17.4	1.1	-0.96	N	16.31	0.84 ± 0.18	> 0.76	?		
50	G	07 18 05.30	-13 18 24.8	17.0	U	13.8	0.9	-2.40	C	14.37	0.42 ± 0.06	0.03 ± 0.08	Y	GK	
50	H	07 18 05.20	-13 18 23.1	19.2	2			> -0.32		14.78	0.16 ± 0.09	0.24 ± 0.17	Y		
51	A	07 18 07.78	-13 20 11.4	14.2	U	17.7	0.7	-0.97	N						
51	B	07 18 08.27	-13 20 16.0	15.2	T	11.4	0.8	-3.94	C	9.87	0.48 ± 0.04	0.04 ± 0.03	Y	K1	$d \sim 115$ pc, $\log(L_X) \sim 28.2$
51	C	07 18 07.25	-13 19 45.3	18.1	U	16.5	0.6	-1.45	N	14.88	0.28 ± 0.07	0.32 ± 0.10	Y		
51	D	07 18 06.90	-13 19 52.7	18.7	U	17.9	0.9	-0.89	N	16.43	0.82 ± 0.19	0.08 ± 0.28	Y		
51	E	07 18 08.74	-13 19 41.1	19.2	2			> -0.45		15.77	0.59 ± 0.12	0.03 ± 0.19	Y		
51	F	07 18 09.38	-13 19 51.2	19.5	U	16.8	0.3	-1.33	N	14.93	0.51 ± 0.06	-0.10 ± 0.12	Y		
51	G	07 18 07.51	-13 20 15.9	20.0	2			> -0.45		16.28	> 1.49		?		
52	A	07 18 11.18	-13 22 45.4	8.6	U	14.4	1.9	-2.00	C	12.23	0.63 ± 0.04	0.25 ± 0.03	Y	M	
52	B	07 18 11.35	-13 22 27.9	13.0	U	17.7	0.8	-0.68	E	15.88	0.46 ± 0.13	± 0.24	Y		
52	C	07 18 09.91	-13 22 48.4	16.6	U	18.0	0.6	-0.56	E	16.33	0.82 ± 0.16	0.17 ± 0.25	Y		
52	D	07 18 12.02	-13 22 33.2	18.2	U	18.0	1.0	-0.56	E	16.49	> 0.44		?		
53	A	07 18 12.57	-13 06 18.3	17.3	U	15.9	0.9	-1.70	N	14.37	0.41 ± 0.05	0.06 ± 0.07	Y	GK	
53	B	07 18 11.25	-13 06 22.2	17.7	2			> -0.46		16.11	0.43 ± 0.17	> 0.86	?		
54	A	07 18 13.78	-13 27 12.2	13.7	2			> -0.12		15.89	0.33 ± 0.36	> 1.15	?		

Table 4 – *continued*

Des.	RA	Dec.	Sep.	Ref.	m_{opt}	Col.	$[f_X/f_{\text{opt}}]$	Cl.	J	$(J - H)$	$(H - K_S)$	MS	Sp.	Notes	
54	B	07 18 13.74	-13 27 15.8	15.7	U	14.1	1.4	-2.08	C	13.36	0.60 ± 0.04	0.12 ± 0.04	Y	K	
55	A	07 18 12.96	-13 23 58.5	6.1	S			-0.20							Radio, [CGN 99] 7
55	B	07 18 13.68	-13 24 03.0	10.0	U	17.3	0.8	-0.20	E	15.43	0.53 ± 0.09	0.34 ± 0.13	Y		
55	C	07 18 15.24	-13 24 08.1	31.5	T	12.4	0.3	-2.63	N	11.88	0.10 ± 0.04	0.03 ± 0.04	Y	A8	$d \sim 1000$ pc, $\log(L_X) \sim 31.0$, prob. too luminous for spectral type
56	A	07 18 38.67	-13 01 29.6	14.2	U	18.9	0.4	-0.17	E	16.41	0.71 ± 0.20	0.46 ± 0.25	Y		
56	B	07 18 37.35	-13 01 10.3	17.4	U	17.8	0.8	-0.61	E						
56	C	07 18 37.29	-13 01 20.8	18.1	T	11.9	0.3	-3.44	C	10.59	0.31 ± 0.04	0.11 ± 0.04	Y	G0	$d \sim 320$ pc, $\log(L_X) \sim 29.5$, Tycho colour suggests earlier type
57	A	07 18 43.66	-13 06 49.7	10.2	U	17.3	1.0	-0.78	E	15.69	0.49 ± 0.13	0.32 ± 0.19	Y		
57	B	07 18 43.23	-13 06 52.7	17.0	U	16.3	2.3	-1.18	C	14.69	0.72 ± 0.06	0.22 ± 0.08	Y	KM	
58	A	07 18 47.58	-12 57 21.7	13.2	U	19.0	0.0	-0.18	E						
58	B	07 18 49.40	-12 57 33.5	16.9	U	15.0	0.5	-1.78	N	13.62	0.26 ± 0.05	0.13 ± 0.06	Y	FG	
58	C	07 18 48.42	-12 57 05.2	18.2	2			> -0.18		16.08	0.69 ± 0.17	> 0.38	?		
58	D	07 18 48.18	-12 57 42.1	19.2	U	18.3	0.6	-0.46	E	16.58	0.70 ± 0.24	0.26 ± 0.33	Y		
59	A	07 19 10.52	-13 15 01.5	5.9	T	9.8	0.9	-4.03	C	8.11	0.50 ± 0.03	0.11 ± 0.04	Y	G8III	HD 57083, $d \sim 630$ pc, $\log(L_X) \sim 30.3$ Spurious
59	B	07 19 10.85	-13 14 53.3	8.5	U	16.8	1.9	-0.76	E						
59	C	07 19 09.43	-13 15 09.0	18.1	U	16.2	1.0	-1.00	N						
60	A	07 22 24.78	-15 10 54.3	6.7	2			> -0.05		15.97	0.48 ± 0.14	0.46 ± 0.18	Y		
60	B	07 22 24.60	-15 11 07.0	10.4	2			> -0.05		16.73	0.84 ± 0.21	0.57 ± 0.24	Y		
60	C	07 22 25.48	-15 10 46.3	14.2	2			> -0.05		16.15	0.59 ± 0.15	0.13 ± 0.23	Y		
60	D	07 22 26.28	-15 11 06.2	17.5	T	11.1	0.1	-3.25	C	10.65	0.04 ± 0.03	0.04 ± 0.03	Y	A5	GSC 05966-01399, $d \sim 760$ pc, $\log(L_X) \sim 30.3$, poss. too luminous for spectral type
60	E	07 22 25.19	-15 11 19.2	20.0	U	18.5	-0.1	-0.25	E	16.47	0.71 ± 0.19	0.38 ± 0.23	Y		
61	A	07 22 29.46	-15 04 10.3	8.2	U	15.5	2.6	-1.28	C	12.76	0.62 ± 0.04	0.27 ± 0.04	Y	M	
61	B	07 22 29.08	-15 04 10.2	12.7	2			> 0.12		16.56	> 3.06		?		
61	C	07 22 29.70	-15 03 45.6	19.2	U	15.7	1.7	-1.20	C	14.31	0.69 ± 0.05	0.10 ± 0.06	Y	KM	
62	A	07 23 06.53	-15 17 47.8	18.9	U	16.8	1.7	-0.90	N	15.71	0.56 ± 0.12	-0.12 ± 0.21	Y	KM?	
63	A	07 23 07.31	-14 58 39.2	4.4	U	12.9	1.0	-2.65	C	12.76	0.27 ± 0.04	-0.02 ± 0.05	Y	F	
63	B	07 23 07.57	-14 58 41.9	7.6	2			> 0.21		15.07	0.69 ± 0.15	0.09 ± 0.19	Y		
63	C	07 23 06.50	-14 58 33.2	11.3	U	16.6	0.9	-1.17	N	14.80	0.66 ± 0.06	0.05 ± 0.08	Y	KM	
63	D	07 23 06.71	-14 58 51.9	11.6	U	17.5	0.9	-0.81	E	15.50	0.58 ± 0.10	0.12 ± 0.14	Y	KM?	
63	E	07 23 08.12	-14 58 41.6	15.6	U	13.4	1.8	-2.45	C	11.60	0.66 ± 0.03	0.21 ± 0.04	Y	M	
64	A	07 23 14.64	-14 52 49.8	1.8	2			> -0.02		14.72	0.38 ± 0.13	0.11 ± 0.14	Y	FGK?	
64	B	07 23 13.91	-14 52 45.7	12.2	T	8.7	0.6	-4.62	C	7.51	0.23 ± 0.05	0.12 ± 0.05	Y	K0III+	HD 58032, $d \sim 400$ pc, $\log(L_X) \sim 29.7$, poss. RS CVn
64	C	07 23 14.44	-14 53 04.2	13.1	U	14.4	2.8	-1.86	C						
64	D	07 23 15.47	-14 52 43.9	15.1	U	15.7	1.7	-1.34	C						
64	E	07 23 15.66	-14 53 00.2	18.2	2			> -0.02		16.31	0.56 ± 0.21	0.69 ± 0.24	N		
65	A	07 23 31.12	-15 12 19.0	2.1	U	10.9	1.0	-3.15	C	10.26	0.25 ± 0.04	0.04 ± 0.04	Y	F	
65	B	07 23 30.37	-15 12 26.2	10.9	U	15.4	1.6	-1.35	C	16.09	> 1.22		?		

Table 4 – continued

Des.	RA	Dec.	Sep.	Ref.	m_{opt}	Col.	$[f_X/f_{\text{opt}}]$	Cl.	J	$(J - H)$	$(H - K_S)$	MS	Sp.	Notes	
66	A	07 23 33.91	-15 10 25.6	10.8	T	9.9	0.9	-4.47	C	8.37	0.47 ± 0.04	0.14 ± 0.04	Y	K2	GSC 05966-00677, $d \sim 50$ pc, $\log(L_X) \sim 27.6$
67	A	07 23 40.61	-16 07 54.5	14.9	U	15.5	2.6	-1.30	C	12.76	0.59 ± 0.04	0.28 ± 0.04	Y	M	
68	A	07 24 01.10	-16 11 54.1	15.7	U	17.2	1.6	-1.04	N						
68	B	07 24 02.07	-16 11 55.7	16.0	U	16.7	1.4	-1.24	N						
68	C	07 24 02.98	-16 11 36.2	19.2	U	16.7	0.6	-1.24	N						
68	D	07 24 01.35	-16 11 21.4	19.9	U	14.2	-0.7	-2.24	N						
69	A	07 24 02.11	-15 05 14.7	13.1	U	18.1	-0.1	-0.39	E	16.48	> -0.54		N		
70	A	07 24 03.24	-14 57 07.7	8.9	2			> -0.16		15.57	0.48 ± 0.11	-0.04 ± 0.31	Y		
70	B	07 24 03.22	-14 57 04.9	11.6	U	15.1	1.1	-1.72	N	14.78	0.49 ± 0.07	0.06 ± 0.10	Y	K	
70	C	07 24 03.45	-14 57 29.6	13.5	U	17.1	1.6	-0.92	N	13.44	0.63 ± 0.04	0.25 ± 0.05	Y	M	
70	D	07 24 04.33	-14 57 24.7	15.5	U	13.9	1.2	-2.20	C	13.67	0.20 ± 0.05	0.07 ± 0.05	Y	F	
71	A	07 24 08.08	-14 59 29.4	1.8	U	18.5	0.4	-0.29	E						
71	B	07 24 08.39	-14 59 34.4	5.5	U	19.2	-0.2	-0.01	E						
71	C	07 24 07.63	-14 59 36.4	10.8	U	16.0	0.5	-1.29	N	15.03	0.55 ± 0.08	0.05 ± 0.13	Y	KM	
71	D	07 24 07.93	-14 59 14.4	15.7	U	15.1	1.0	-1.65	N	14.15	0.32 ± 0.05	0.07 ± 0.08	Y	FG	
71	E	07 24 07.21	-14 59 22.6	16.1	U	16.2	0.8	-1.21	N	15.28	± 0.12	0.41 ± 0.18	N		
71	F	07 24 07.15	-14 59 37.5	17.2	U	16.8	0.4	-0.97	N	15.64	0.08 ± 0.16	0.61 ± 0.22	N		
71	G	07 24 08.83	-14 59 13.2	18.7	U	16.9	0.8	-0.93	N	15.83	0.29 ± 0.14	0.20 ± 0.23	Y		
72	A	07 25 18.58	-16 10 22.9	12.6	U	16.7	1.2	-0.53	E	16.01	0.52 ± 0.16	> -0.36	N		
72	B	07 25 17.35	-16 10 41.9	16.0	U	18.9	1.0	0.35	E	16.52	> -0.80		N		
72	C	07 25 18.21	-16 10 53.8	18.9	2			> 0.39		16.71	> 1.18	< 0.14	?		
73	-							> 0.23	U						No optical or near-IR counterpart
74	A	08 09 24.27	-33 29 53.9	7.5	U	17.8	1.2	-0.20	E						
74	B	08 09 23.46	-33 30 12.3	13.5	U	17.9	2.3	-0.16	E						
74	C	08 09 24.13	-33 30 15.5	14.9	U	18.0	1.8	-0.12	E						
74	D	08 09 24.98	-33 30 09.6	15.2	T	12.2	0.6	-2.92	C	10.96	0.32 ± 0.04	0.09 ± 0.04	Y	G2	$d \sim 320$ pc, $\log(L_X) \sim 29.8$
74	E	08 09 25.20	-33 30 03.4	15.2	2			> 0.28		15.92	0.23 ± 0.18	> 1.06	?		
74	F	08 09 24.42	-33 29 45.1	16.4	U	15.3	0.2	-1.20	N	14.59	0.18 ± 0.07	0.14 ± 0.10	Y	F	
75	A	08 09 26.36	-33 20 17.4	2.2	U	17.8	0.7	-0.38	E	16.59	> 0.44		?		
75	B	08 09 26.54	-33 20 11.1	4.9	U	18.0	1.8	-0.30	E						
75	C	08 09 27.32	-33 20 10.4	13.3	U	17.2	0.7	-0.62	E	16.05	0.38 ± 0.16	> 0.73	?		
75	D	08 09 25.20	-33 20 18.5	13.6	T	12.2	0.2	-3.08	N	10.81	0.20 ± 0.04	0.02 ± 0.04	Y	F2	CD-32 4913, $d \sim 580$ pc, $\log(L_X) \sim 30.2$, poss. too luminous for spectral type
75	E	08 09 25.11	-33 20 10.6	16.0	2			> 0.10		16.07	0.23 ± 0.24	> 1.31	?		
75	F	08 09 25.23	-33 20 06.7	16.2	2			> 0.10		15.86	0.28 ± 0.17	> 0.51	?		
75	G	08 09 25.81	-33 20 34.7	20.5	U	15.3	0.9	-1.38	N	15.25	0.38 ± 0.11	0.13 ± 0.14	Y		
76	A	08 09 27.28	-33 25 09.9	7.9	U	16.6	0.6	-0.73	E	15.58	0.50 ± 0.10	-0.13 ± 0.20	Y	?	
76	B	08 09 26.03	-33 25 07.6	14.6	U	17.8	0.9	-0.25	E						
76	C	08 09 28.14	-33 25 14.8	15.0	U	18.0	2.1	-0.17	E						
76	D	08 09 25.46	-33 25 10.8	19.6	U	17.0	1.1	-0.57	E	15.62	0.64 ± 0.11	0.04 ± 0.17	Y	KM?	
76	E	08 09 28.39	-33 25 25.1	19.9	U	17.9	2.5	-0.21	E						

Table 4 – *continued*

Des.	RA	Dec.	Sep.	Ref.	m_{opt}	Col.	$[f_X/f_{\text{opt}}]$	Cl.	J	$(J - H)$	$(H - K_S)$	MS	Sp.	Notes
77	A	08 10 18.00	-33 06 11.1	5.4	U	17.0	0.8	-0.87	N	15.26	0.53 ± 0.08	0.26 ± 0.12	Y	?
77	B	08 10 18.35	-33 06 00.8	9.5	U	17.9	1.2	-0.51	E	16.45	0.26 ± 0.26	>0.25	?	
77	C	08 10 19.41	-33 06 12.1	12.5	U	14.7	1.6	-1.79	C	12.05	0.69 ± 0.04	0.26 ± 0.04	Y	M
77	D	08 10 17.17	-33 06 05.9	16.3	U	18.0	2.4	-0.47	E					
77	E	08 10 19.97	-33 06 10.7	19.5	U	17.6	1.0	-0.63	E	16.02	0.51 ± 0.15	>0.28	?	
77	F	08 10 17.66	-33 05 52.3	20.4	U	17.9	2.5	-0.51	E	15.98	0.69 ± 0.13	0.37 ± 0.18	Y	
78	A	10 22 59.10	-57 42 44.0	3.7	U	17.9	0.6	-0.28	E					
78	B	10 23 00.43	-57 42 42.2	7.8	U	16.5	1.7	-0.84	N					
78	C	10 22 58.43	-57 42 37.3	9.3	U	14.0	2.4	-1.84	C					
78	D	10 23 00.09	-57 42 32.2	10.6	U	16.3	0.8	-0.92	N					
78	E	10 23 00.82	-57 42 33.5	13.6	U	15.6	1.1	-1.20	N					
78	F	10 22 59.77	-57 42 55.9	14.6	U	17.1	0.5	-0.60	E					
78	G	10 22 59.16	-57 43 00.5	19.0	U	15.3	0.9	-1.32	N					
79	A	10 23 38.96	-57 58 05.0	5.0	U	12.4	0.3	-2.60	N					
79	B	10 23 39.87	-57 57 44.7	17.5	U	16.5	0.7	-0.96	N					
80	A	10 23 44.50	-57 38 31.6	6.9	T	9.1	0.1	-4.35	C				O7	HD 90273, prob. highly reddened Spurious
80	B	10 23 44.49	-57 38 47.5	15.3	U	17.1	-4.2	-0.68	E					
81	A	10 23 51.90	-57 58 01.7	20.0	U	13.9	4.2	-2.05	C					
81	B	10 23 50.64	-57 57 14.1	30.2	T	6.3	1.5	-5.54	C				K4III	NSV 4846, $d \sim 180$ pc, $\log(L_X) \sim 29.0$, beyond coronal dividing line
82	A	10 23 58.1	-57 45 49		S									Open cluster Westerlund 2
83	A	10 24 14.75	-57 39 51.7	5.2	U	17.7	2.4	-0.69	E					
83	B	10 24 14.35	-57 39 43.6	5.9	U	16.9	1.2	-1.01	N					
83	C	10 24 12.77	-57 39 42.3	18.2	U	17.7	2.0	-0.69	E					
84	A	10 24 46.80	-57 32 58.8	5.0	U	16.4	0.7	-1.16	N					
84	B	10 24 48.32	-57 32 50.2	10.2	U	14.3	0.7	-2.00	N					
84	C	10 24 47.55	-57 32 37.3	17.8	U	17.7	1.7	-0.64	E					
84	D	10 24 45.42	-57 33 06.2	18.2	U	17.7	1.2	-0.64	E					
85	A	10 25 01.16	-57 54 29.5	5.4	U	17.4	1.9	-0.78	E					
85	B	10 25 01.91	-57 54 34.4	9.9	U	17.7	2.1	-0.66	E					
85	C	10 25 01.38	-57 54 13.3	11.6	U	15.0	0.5	-1.74	N					
85	D	10 25 03.00	-57 54 21.1	12.3	U	14.1	0.8	-2.10	N					
85	E	10 25 02.87	-57 54 38.6	17.4	U	16.4	0.8	-1.18	N					
85	F	10 25 01.52	-57 54 43.9	19.9	U	15.9	0.9	-1.38	N					
86	A	10 25 34.78	-57 50 40.3	10.8	U	17.6	0.5	-0.50	E					
86	B	10 25 37.00	-57 50 43.9	16.7	U	15.3	0.0	-1.42	N					
87	A	10 25 45.65	-57 35 34.8	3.9	U	17.6	1.9	-0.19	E					
87	B	10 25 44.95	-57 35 26.7	6.6	U	16.2	0.4	-0.75	E					
87	C	10 25 45.32	-57 35 40.1	9.4	U	16.1	0.7	-0.79	E					
87	D	10 25 46.67	-57 35 22.5	12.2	U	14.6	1.9	-1.39	C					
87	E	10 25 47.53	-57 35 29.8	15.7	U	17.2	0.3	-0.35	E					
87	F	10 25 47.55	-57 35 22.1	18.2	U	16.6	2.3	-0.59	E					
87	G	10 25 43.79	-57 35 18.6	19.0	U	16.6	1.2	-0.59	E					

Table 4 – *continued*

Des.	RA	Dec.	Sep.	Ref.	m_{opt}	Col.	$[f_{\chi}/f_{\text{opt}}]$	Cl.	J	$(J - H)$	$(H - K_S)$	MS	Sp.	Notes
88	A	10 25 53.51	-57 53 57.8	9.7	U	14.7	1.4	-1.81	C					
88	B	10 25 51.66	-57 53 50.5	10.9	U	17.9	1.2	-0.53	E					
88	C	10 25 53.70	-57 53 49.4	15.2	U	17.0	-0.2	-0.89	N					
88	D	10 25 54.13	-57 54 05.9	15.5	U	17.6	-0.5	-0.65	E					
88	E	10 25 52.27	-57 54 15.9	15.9	U	15.8	0.3	-1.37	N					
88	F	10 25 53.93	-57 53 45.4	19.4	U	17.2	1.5	-0.81	E					
89	A	10 25 53.36	-57 37 57.5	8.1	U	17.0	0.1	-0.69	E					
89	B	10 25 53.85	-57 38 04.7	8.4	U	17.2	0.6	-0.61	E					
89	C	10 25 52.92	-57 37 48.7	14.5	U	17.6	0.7	-0.45	E					
89	D	10 25 56.05	-57 37 47.6	16.6	U	12.4	3.2	-2.53	C					
89	E	10 25 55.64	-57 38 10.8	16.8	U	16.9	1.4	-0.73	E					
89	F	10 25 52.34	-57 38 07.9	19.4	U	18.0	1.7	-0.29	E					
89	G	10 25 56.82	-57 37 56.9	19.7	U	14.0	-2.0	-1.89	N					
90	A	10 25 54.20	-57 48 43.4	11.6	U	16.0	-0.5	0.33	E					
90	B	10 25 56.51	-57 48 43.4	14.1	U	11.6	1.4	-1.43	N				WR	WACK 2134, $\log(f_{\chi}/f_{\text{opt}})$ high for early-type star
90	C	10 25 56.25	-57 49 04.7	15.3	U	17.8	0.7	1.05	E					
90	D	10 25 53.23	-57 48 44.3	17.1	U	17.8	0.7	1.05	E					
90	E	10 25 53.45	-57 49 04.6	18.2	U	17.6	0.1	0.97	E					
91	A	10 26 02.91	-57 59 11.1	5.9	U	17.7	2.4	0.50	E					
91	B	10 26 04.37	-57 59 19.1	8.5	U	17.7	1.0	0.50	E					
91	C	10 26 03.10	-57 59 27.1	11.8	U	14.0	0.9	-0.98	N					
91	D	10 26 03.10	-57 59 27.1	14.0	U	17.8	1.5	0.54	E					
91	E	10 26 01.42	-57 59 05.9	18.4	U	18.0	1.1	0.62	E					
92	A	10 26 05.01	-57 46 37.1	7.5	U	17.0	-0.1	-0.91	N					
92	B	10 26 03.44	-57 46 28.4	11.5	U	15.7	-0.2	-1.43	N					
92	C	10 26 02.54	-57 46 29.8	15.2	U	17.9	1.0	-0.55	E					
92	D	10 26 06.18	-57 46 37.2	16.8	U	14.7	1.4	-1.83	C					
92	E	10 26 04.83	-57 46 22.4	17.2	U	11.9	1.2	-2.95	C					
92	F	10 26 03.34	-57 46 57.2	19.6	U	12.6	1.9	-2.67	C					
93	A	10 26 09.98	-57 56 59.6	10.0	U	17.8	1.2	0.01	E					
93	B	10 26 10.77	-57 56 45.4	10.8	U	17.8	1.5	0.01	E					
93	C	10 26 11.18	-57 56 43.9	11.9	U	17.7	2.0	-0.03	E					
93	D	10 26 12.08	-57 57 05.4	12.2	U	17.1	1.2	-0.27	E					
93	E	10 26 12.60	-57 56 45.8	15.3	U	15.0	1.5	-1.11	N					

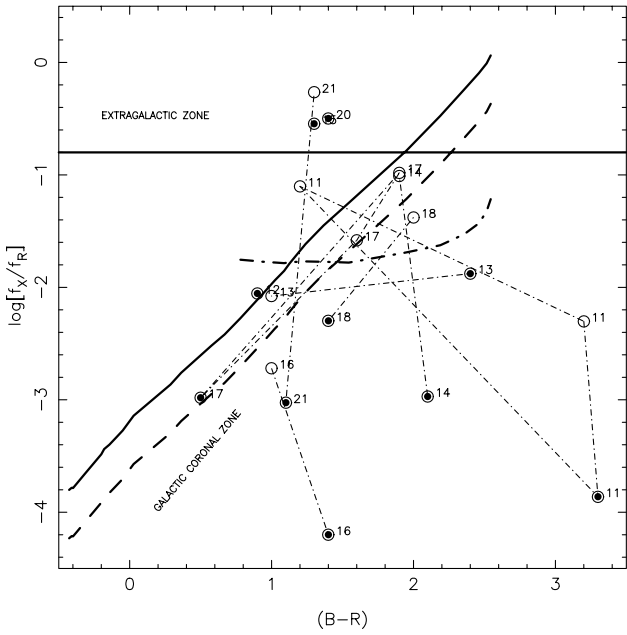


Figure 6. Plot of $\log(f_X/f_R)$ versus $B-R$ for all potential optical counterparts to X-ray sources in field 2 found in the USNO-A2.0 catalogue. The plotted quantities are not corrected for reddening or absorption. The coronal and extragalactic boundaries and the saturation threshold are indicated using the same bold lines as in Fig. 5. Fine dot-dashed lines join candidate counterparts to the same X-ray source. A filled circle indicates the counterpart found deepest in the coronal zone, or the brightest counterpart where there is no coronal counterpart.

5.1 X-ray to optical flux ratio

We have an optical magnitude (either V from Tycho-2, or R from USNO-A2.0) for the majority of our candidate counterparts and can compute upper limits ($R > 19$) for those found only in 2MASS, enabling us to calculate the X-ray to optical flux ratio for each candidate. This parameter is useful in attempts to identify and classify X-ray sources.

To convert X-ray count rate C_X (units: PSPC hard-band counts s^{-1}) to flux f_X (units: $\text{erg cm}^{-2} \text{s}^{-1}$) in the nominal energy band 0.4–2 keV, we assume

$$f_X = 1.0 \times 10^{-11} C_X,$$

and for the optical (V -band) flux, f_V (units: $\text{erg cm}^{-2} \text{s}^{-1} \text{\AA}^{-1}$),

$$\log f_V = -0.4m_V - 8.43$$

(e.g. Allen 1973). Hence

$$\log(f_X/f_V) = \log(C_X) + 0.4m_V - 5.52,$$

where $\log f_V$ is now integrated over the 890 \AA V -band width. The calculation for the POSS-I E (red: $\lambda_0 \approx 6500 \text{\AA}$) plate flux is very similar:

$$\log f_R = -0.4m_R - 8.65.$$

Hence

$$\log(f_X/f_R) = \log(C_X) + 0.4m_R - 5.05,$$

where $\log f_R$ is now integrated over the approximately 500 \AA E -plate band width.

Extensive X-ray surveys, e.g. EMSS (Stocke et al. 1991) and RGPS (Motch et al. 1998), have found that, except at the high end of the flux distribution, the soft X-ray source populations are dominated by two classes: active coronae and active galactic nuclei (AGN). These surveys have also found that these two classes of objects are readily separated on the basis of their X-ray to optical flux ratios. In general, AGN have $\log(f_X/f_V) > -1$ while active coronae have $\log(f_X/f_V) < -1$. Furthermore, active coronae show a saturation limit of X-ray luminosity at $\sim 10^{-3}$ of their bolometric luminosity so that earlier-type stars have more stringent limits upon their X-ray to optical flux ratio. This is well demonstrated in the EMSS results (Stocke et al. 1991, fig. 7), which plot $\log(f_X/f_V)$ versus $(B-V)$. We have formed approximate 90 and 98 per cent upper limits for coronal sources from this figure, which can be used to discriminate between coronal and non-coronal sources. Note that the EMSS boundary does not directly reflect the saturation limit of active coronae. If we calculate $\log(f_X/f_V)$ for saturated main-sequence (MS) stars from bolometric corrections (Schmidt-Kaler 1982) and plot this against $(B-V)$ (using MS colours of Johnson 1966) we find this ‘saturation boundary’ crosses the EMSS boundary at spectral type $\sim K0$ and has a much shallower slope until the M-type stars, when it steepens to a similar slope as the EMSS boundary, below which the saturation boundary remains by approximately one dex. This implies that a fraction of the EMSS sample (~ 5 –10 per cent) was detected while emitting above their nominal saturation limit, and we may expect some fraction of our sources also to be active coronae emitting above this limit, but still to be contained by the EMSS boundary (see Fig. 5).

5.1.1 Tycho-2

Given the flux limit of our survey and the magnitude limit of Tycho-2, we would expect all the counterparts found in this catalogue to be stars, and the majority of these to be active coronae. We have plotted these on a diagram of $\log(f_X/f_V)$ versus $(B-V)$ to verify this and perhaps identify cases in which the Tycho-2 star

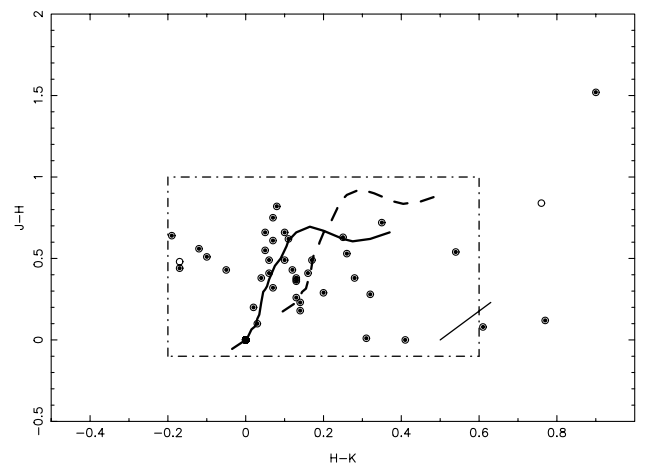


Figure 7. Near-infrared two-colour diagram for N-type sources (as classified in Figs 5 or 6), found in the 2MASS Second Incremental Data Release. Open circles indicate non-detections in the K_S band. The bold line shows the main-sequence (MS) locus of Bessell & Brett (1988), while the bold dashed line shows the same locus reddened by absorption of $A_V = 2$. This reddening vector is also shown. We used the dot-dashed box to define objects that were consistent with being MS stars. Note that the majority of these objects are consistent with being MS stars.

is inconsistent with being an active corona (and hence is probably not the actual identification of the X-ray source).

Note that the EMSS and saturated boundaries assume zero absorption in the X-ray and optical and hence zero reddening, while we have plotted the observed reddened magnitudes and absorbed fluxes. Since the ratio of X-ray to optical flux is little affected by absorbing columns with $N_{\text{H}} \lesssim 10^{21} \text{ cm}^{-2}$, and the optical absorption dominates over the X-ray attenuation for higher columns, we expect a plotted point to lie at higher $\log(f_{\text{X}}/f_{\text{V}})$ than its intrinsic position (Briggs et al. 2000). However, $B - V$ also increases with increasing absorption, and the slope of the reddening vector in the diagram is shallower than the slope of the EMSS boundary, so we do not expect any true coronal source to fall outside the ‘coronal zone’. If we assume a reasonable absorption ($A_{\text{V}} \leq 1.5 \text{ mag kpc}^{-1}$), we estimate that the most luminous coronal source ($L_{\text{X}} \approx 10^{31} \text{ erg s}^{-1}$) could not be detected in our survey through a column higher than $\sim 4 \times 10^{21} \text{ cm}^{-2}$, implying a shift in $\log(f_{\text{X}}/f_{\text{V}})$ of no more than 0.5, and much smaller for less luminous sources. The mean error in the PSPC count rates is 25 per cent, which corresponds to ± 0.1 in $\log(f_{\text{X}}/f_{\text{V}})$, and the Tycho-2 photometric errors of $\leq \pm 0.1 \text{ mag}$ give errors of ± 0.04 in $\log(f_{\text{X}}/f_{\text{V}})$.

When we plot the 19 Tycho-2 sources on this diagram (Fig. 5), only the counterparts to sources 55 and 75 fall outside the coronal zone. Both are within the errors, noted above, of the boundary, but we note that the candidate for source 55 is one of the two found more than 20 arcsec from its X-ray source.

5.1.2 USNO-A2.0

We encounter two problems in performing the same test using USNO photometry. First, the blue and red magnitudes are photographic magnitudes that only roughly approximate to Johnson B - and R -band magnitudes. Fields 1–7 are covered by POSS-I O and E plates, while the southerly fields 8 and 9 are covered by the SRC J and ESO-R F plates, although the photometric solutions in the USNO-A2.0 catalogue do not account for bandpass differences between the two sets of red or blue plates. Therefore, we use the POSS-I bandpasses here. Humphreys et al. (1991) determined the colour transformations $O - B$ and $E - R$ as functions of $B - V$ and $V - R$ respectively. $O - B$ is a very weak function of $B - V$ and has the small range of 0–0.2 for mid- and late-type stars ($B - V > 0$), which is within the quoted USNO-A2.0 photometric errors, so we make the approximation $O \approx B$. E can be transformed using the relation

$$E - R = -0.011 + 0.148(V - R) + 0.058(V - R)^4$$

for $-0.2 < V - R < 1.7$. The relation is flatter at redder colours.

We transformed the coronal boundary by using this relation and the mean intrinsic colours for main-sequence stars (i.e. $V - R$ versus $B - V$) measured by Johnson (1966). We converted the extragalactic boundary by applying the measured mean ($V - R$) for a sample of bright radio galaxies (Machalski & Wiśniewski 1988) of $+0.91 (\pm 0.12)$, shifting the boundary to $\log(f_{\text{X}}/f_{\text{R}}) = -0.8$. Secondly, the USNO photometry is not well constrained. The reported accuracy is $\pm 0.2 \text{ mag}$, but there are a number of cases where we see discrepancies much greater than this. While this does not strongly affect the accuracy of $\log(f_{\text{X}}/f_{\text{R}})$, it can make the $B - R$ colour unreliable. This is a strong motivation for using the 2MASS catalogue for photometric information where available.

We plotted the counterparts on a diagram of $\log(f_{\text{X}}/f_{\text{R}})$ versus $B - R$, one field at a time, and classified each according to the region [‘extragalactic’ (E), ‘coronal’ (C) or ‘neither’/‘no man’s land’ (N)] into which it fell. We only show the diagram for field 2 here (Fig. 6), as the many potential counterparts in some fields make the diagrams very crowded. Many candidates fell in the ‘extragalactic’ zone, which is not unexpected: while we expect most true AGN to be so heavily absorbed as to be undetectable in the optical ($V \sim 19$ – 24), many faint background stars that fall into the error circles by chance and are not associated with a detected X-ray source should fall in this region of the diagram. A surprisingly high number of bright counterparts fell into ‘no man’s land’. The only sources we expect to find in this region are the easily absorbed white dwarfs and the comparatively sparse accreting binaries.

Accepting the BM94 identification of three sources with (non-coronal) early-type stars, 50 sources were found to have ‘coronal’ candidates, one of which SIMBAD reveals to be a compact H II region. Considering the brightest candidates to the remaining sources, 25 were classed ‘no man’s land’, 12 ‘extragalactic’, with three unidentified.

The larger-than-expected number of ‘no man’s land’ objects may be due to (a) a fainter counterpart being the correct identification, (b) an unrecognised population of low f_{X} X-ray sources or (c) inaccurate (too blue) colours in the USNO-A2.0 catalogue. Fainter counterparts would mean higher $\log(f_{\text{X}}/f_{\text{R}})$ and point to an unreasonably large number of extragalactic detections. We have used 2MASS near-IR colours to indicate whether candidates are consistent with being MS stars, and hence highlight unusual objects or inaccurate $B - R$ values.

5.2 Near-infrared two-colour diagram

We plotted all 2MASS potential counterparts on a $J - H$ versus $H - K_{\text{S}}$ diagram, upon which we superimposed an empirical locus for MS stars (from Bessell & Brett 1988⁶) and defined a box region (from consideration of the quoted photometric errors) within which objects could be considered consistent with being MS stars⁷ (Fig. 7). The 2MASS data have given some insight into whether objects that fell into the ‘N’ region of the $\log(f_{\text{X}}/f_{\text{R}})$ versus $B - R$ diagram did so because of errors in the USNO colours, or because they are not coronal sources. Of the 14 sources whose brightest and/or reddest counterparts fell in ‘no man’s land’ and were covered in the 2MASS Second Incremental Data Release, seven have near-IR colours consistent with being MS stars and $\log(f_{\text{X}}/f_{\text{R}})$ values consistent with active coronae, strongly suggesting that the errors are in the USNO colours and most of the ‘N’ class sources are actually coronal (see Fig. 7).

For objects within photometric error of the MS locus and with $\sigma_{J-H} \leq 0.1$, we have estimated the spectral type by comparing primarily $J - H$ and secondarily $H - K_{\text{S}}$ colours (not accounting for any possible reddening – the reddening vector for $A_{\text{V}} = 2$ is shown in Fig. 7) to the MS near-IR colour tables

⁶Fortuitously the 2MASS colours are well matched to the Bessell & Brett colours.

⁷The locus for giant stars does not diverge from the MS locus until K5III, which is beyond the coronal dividing line (Ayres et al. 1981; Haisch & Simon 1982), so we do not expect to exclude any X-ray emitting giant sources. This box region is consistent with the spread observed by Finlator et al. (2000), with an allowance for reddening equivalent to $A_{\text{V}} = 2$.

Table 5. Criteria for defining spectral type via 2MASS colours [adapted from the colour tables of Bessell & Brett (1988)]. The effects of reddening are not included. Note that the class labelled ‘km?’ has $J - H$ lower than M-type stars but $H - K_S$ higher than K-type stars. This could be due to reddening or to scatter in $J - H$ or $H - K_S$. These objects have been tentatively classed with the M-type stars in Fig. 8.

Spectral type	$J - H$	$H - K_S$
A	0.00–0.10	<0.15
F	0.10–0.30	<0.15
G	0.30–0.40	<0.15
K0–K2	0.40–0.50	<0.15
K2–K7	0.50–0.80	<0.15
km?	0.50–0.60	>0.15
M	0.60–0.80	>0.15
gM	>0.80	>0.15

of Bessell & Brett (1988).⁸ The classification criteria are shown in Table 5. Candidate counterparts to source 11 (the H II region) have been excluded. The sample includes 83 potential counterparts to 47 X-ray sources. Fig. 8 shows the distribution of this sample by estimated spectral type. A crude attempt has also been made to weight each counterpart according to its likelihood of being the correct identification for the X-ray source. This judgment was made on the bases of optical brightness (probability that an object of that brightness would appear within 20 arcsec of an X-ray source position by chance alone) and $\log(f_X/f_{\text{opt}})$ versus estimated spectral type. Each candidate was given a weighting from 0 to 1 in grades of 0.2 such that the sum of weightings for all candidates to any particular X-ray source was 1. The resultant distribution among spectral types is shown in Fig. 8 using a dashed line. There are no major differences between the total and weighted distributions. K-type stars are the most frequent counterparts. We estimate that ~ 12 sources are M-type stars, although the photometric selection criteria of the sample do bias against the least-luminous spectral type.

To investigate the USNO colours further, we took all the matches within 2 arcsec between 2MASS and USNO-A2.0 catalogues in a single field, estimated spectral types exactly as above, and compared the distribution of USNO colour for each spectral type with the expected range of these colours. F stars peaked ~ 0.2 mag lower than the expected minimum, but had a long tail extending to $B - R \sim 3$. G stars peaked ~ 0.5 mag lower than expected, with a sharp low cut-off at 0.2 and a steady slope to ~ 3.5 . This indicates that the mean for F and G stars is actually *much higher* than expected, although the rms scatter is 1 mag. The K-star distribution was more Gaussian, with a peak and mean within the expected range, with rms spread of 1 mag. The M-star distribution was also more Gaussian-like, with a mean in the expected range and rms scatter of 0.7 mag, and a fairly sharp lower cut-off around 1.3. The expected effect of reddening is for the true spectral type to be *earlier* than estimated, yet for $B - R$ to be still *higher* than appropriate for the estimated spectral type. Heavy reddening may

⁸ Finlator et al. (2000) conclude that spectral types cannot be accurately estimated from 2MASS colours alone, although stars later than K5 are well separated from those earlier than G5.

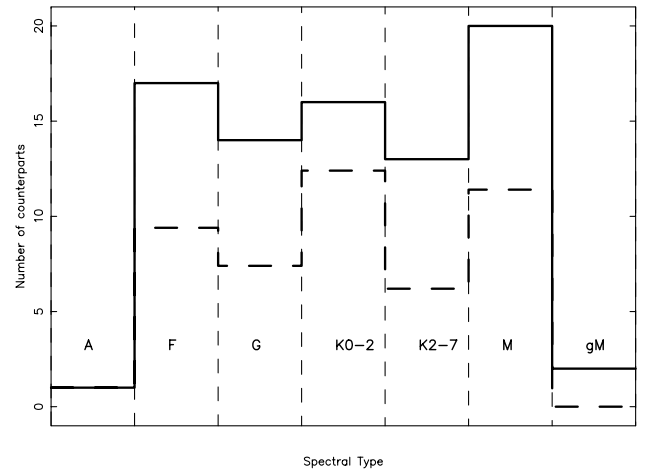


Figure 8. Histogram of spectral types estimated by comparison of 2MASS photometry to the MS near-IR colour tables of Bessell & Brett (1988). The classification criteria are shown in Table 5. Only objects within photometric error of the MS locus and $\sigma_{J-H} \leq 0.1$ are included in the sample of 83 candidates to 47 X-ray sources. The solid line includes all 83 counterparts; the dashed line is weighted such that each X-ray source contributes 1 to the sample (see text for details).

explain the long tails on the F and G distributions. While this indicates that objects certainly *may* have colours that are significantly too blue for their spectral type, it does not point towards a systematic trend.

We have estimated the X-ray luminosity of those sources with counterparts in the Tycho-2 catalogue that have published spectral types or spectral types estimated from well-constrained 2MASS colours ($\sigma_{J-H} \leq 0.1$). A distance modulus (not corrected for absorption) was calculated for each star using the absolute magnitudes of Schmidt-Kaler (1982), which was converted into a distance used to calculate the (0.4–2.0 keV) X-ray luminosity from the hard-band flux listed in Table 2. These estimated distances and luminosities are listed in the final column of Table 4. The neglect of absorption in this procedure may underestimate the true luminosity, but this should be a small problem in the hard band. The high luminosity of source 55 [$\log(L_X) \sim 31.0$ erg cm⁻² s⁻¹] if 55C is the counterpart rules out this late A-type star as a candidate (recall it was also > 30 arcsec from the source position).

The bulk of 2MASS galaxies in off-plane directions are found with $0.2 \leq (H - K_S) \leq 0.6$ and $0.6 \leq (J - H) \leq 0.9$ (Cutri et al. 2000). As the typical column through the Galaxy in each field of $N_H \sim 10^{22}$ cm⁻² implies $A_V \sim 5$ mag, we would expect any galaxies among our counterparts to sit well above and to the right of the MS locus. None of our ‘extragalactic’ candidates actually occupies this part of the two-colour diagram, which suggests that they are chance associations with stars rather than the true optical counterparts, which must be fainter and hence have higher $\log(f_X/f_R)$. Indeed, many of the ‘extragalactic’ candidates have 2MASS colours consistent with MS stars (see Table 4).

5.3 Hardness ratios

We calculated hardness ratios $HR = (H - S)/(H + S)$ for all 12 sources detected in the soft band (see Table 3). Previous surveys have found such ratios useful in distinguishing between sources of different types (e.g. Motch et al. 1998; Haberl & Pietsch 1999; Haberl et al. 2000). Unabsorbed coronal sources typically have

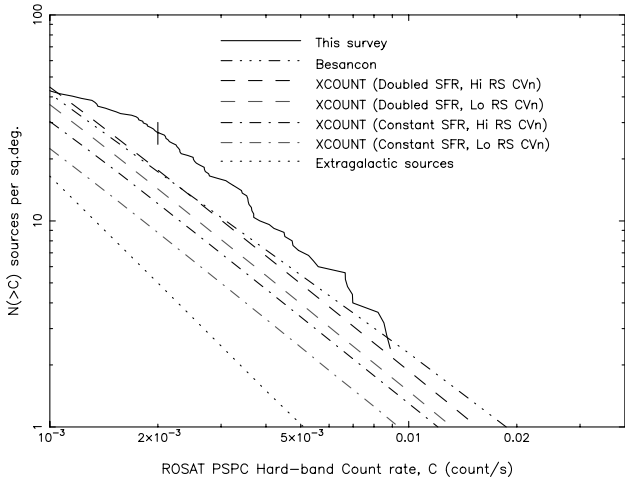


Figure 9. Measured and predicted Galactic plane $\log N$ – $\log S$ relations. From top to bottom, the curves are: (a) our measured, coverage-corrected $\log N$ – $\log S$; (b) prediction of the Besançon model (Guillout et al. 1996a) corrected for hard band; (c)–(f) predictions of the XCOUNT model, with two different assumptions for the star formation rate in the last 10^9 yr and two different assumptions for the density of RS CVn binaries (see Section 6); and (g) estimated contribution from extragalactic sources using a Galactic transmission factor of 0.3 and the high-latitude measurements of Hasinger et al. (1993).

$HR \sim 0$, but can have values significantly higher (if they are heavily absorbed, or flaring) or lower (if they have intrinsically cooler coronae). The hardest source is the flaring source 91. The softest source detected in the hard band is source 16, whose most likely counterpart is the 10th magnitude (possibly G type) star GSC 01318-00940. Three sources were detected only in the soft band. Hot white dwarfs (WDs) are typically very soft sources, but their flux is easily absorbed so they cannot be seen to great distances in heavily obscured regions like the Galactic plane. None of our soft sources has a counterpart with the blue colours expected of a WD, although an X-ray emitting WD could be hidden by an optically brighter companion. Sources 6 and 47 may be such systems, although source 22 is not. We have estimated the only counterpart, 22A, to be a mid-M dwarf. While the X-ray source is much softer ($HR \leq -0.69$) than a typical active dM star, such as 67A (which is very similar photometrically (see Table 4) but has $HR = -0.24$), the dM star is too faint to hide a hot WD in the system.

5.4 Classifying sources

In the crowded region of the Galactic plane, it is nearly impossible to determine the correct counterpart to each X-ray source without good-quality spectra of the candidates, which would require an

extensive optical observing programme. However, we seek to test the hypothesis that the majority of X-ray sources in the Galactic plane are due to coronal emission from late-type stars. Therefore, if there is any object in the X-ray source’s error circle that we may classify as ‘coronal’, we consider that source to be consistent with being coronal. Our classification procedure is as follows.

(i) *Coronal.* A candidate is classed ‘coronal’ if: (a) it falls in the coronal zone of the Tycho-2 $\log(f_X/f_V)$ versus $B - V$ or USNO-A2.0 $\log(f_X/f_R)$ versus $B - R$ diagram and any available 2MASS photometry does not rule out an MS star; or (b) it falls in the ‘no man’s land’ region of the $\log(f_X/f_R)$ versus $B - R$ diagram and 2MASS photometry is consistent with that of an MS star. Where there is no ‘coronal’ candidate, we have taken the classification of the brightest candidate in the error circle.

(ii) *Extragalactic.* A candidate is classed ‘extragalactic’ if: it falls in the extragalactic zone of the $\log(f_X/f_R)$ versus $B - R$ diagram or appears in 2MASS only. Note that the most active late-type stars may be counted as extragalactic if their USNO colours are erroneously blue, but the 2MASS colours should discriminate between the galaxies and the latest-type stars, and any candidates we misclassify in this way must be emitting above their nominal saturation threshold. It is possible that embedded objects, such as protostars, may also be erroneously included in this class. There are several objects around the H II region associated with source 11 that are seen only in 2MASS with very red colours; these are possibly embedded objects, but unlikely to contribute to the X-ray flux of source 11, as the H II region is too distant.

(iii) *No man’s land* candidates are those that fall into that region of the $\log(f_X/f_R)$ versus $B - R$ diagram and have either no or non-MS 2MASS photometry.

(iv) *Other* classifications (e.g. early-type stars, and H II regions) come from SIMBAD, while *Unidentified* sources are those for which we could find no potential counterpart.

5.5 Comparison with previous surveys

The results of this classification method are: 64 (69 per cent) coronal sources, 14 (15 per cent) ‘extragalactic’ sources, 10 (11 per cent) ‘no man’s land’, 4 (4 per cent) ‘other’ sources and 1 (1 per cent) ‘unidentified’. These fractions are unchanged by considering the 90 per cent complete sample with count rates greater than $0.002 \text{ count s}^{-1}$. When we consider that some of the extragalactic and many of the ‘no man’s land’ sources may turn out to be coronal, this result is consistent with extending an order of magnitude fainter in flux the Motch et al. (1997) finding that 85 per cent of the X-ray sources brighter than $0.03 \text{ PSPC count s}^{-1}$ in the Cygnus region of the Galactic plane are due to active coronae. The

Table 6. The relative contribution of each stellar population to the stellar X-ray source counts predicted by various XCOUNT models. Main-sequence stars are modelled in three age ranges: young (0.01–0.1 Gyr), intermediate (0.1–1 Gyr) and old (>1 Gyr). A count-rate threshold of $0.002 \text{ PSPC count s}^{-1}$ has been applied.

Stellar population	Percentage of predicted stellar X-ray sources			
	Constant SFR		Doubled SFR	
	High RS CVn	Low RS CVn	High RS CVn	Low RS CVn
Young	20.8	28.9	28.7	35.4
Intermediate	24.7	34.2	33.9	41.9
Old	15.4	21.4	10.6	13.1
Giants	1.7	2.4	1.2	1.4
RS CVn	37.3	13.3	25.6	8.1

results of our survey are also consistent with earlier high-flux X-ray surveys in the Galactic plane. The *ROSAT* ‘glance’ towards the Perseus Arm (Motch et al. 1991) concluded that ≥ 50 per cent of its observed sources were coronal in origin whilst ≥ 10 per cent were extragalactic, with 40 per cent remaining unidentified. M stars accounted for ≈ 20 per cent of the identified coronal sources and could account for a significant fraction (~ 20 per cent) of the unidentified sources. We have estimated M dwarfs to comprise ~ 25 per cent of the 47 sources in our survey that have coronal counterparts with 2MASS photometry good enough to estimate spectral types. The EGPS (Hertz & Grindlay 1984, 1988) provided similar results, though with a higher extragalactic proportion, probably as a result of their harder energy band.

A number of the coronae seem to have been detected while emitting above their nominal saturation limits. We have taken only those coronal sources for which we have published spectral classifications (SIMBAD) or have estimated spectral types from well-constrained ($\sigma_{J-H} \leq 0.1$) 2MASS colours, and compared their $\log(f_X/f_R)$ values with those expected for saturated [$\log(L_X/L_{\text{bol}}) = -3$] coronal MS stars of the same spectral type. The $\log(f_X/f_R)$ values expected from saturated [$\log(L_X/L_{\text{bol}}) = -3$] coronal MS stars are fairly insensitive to spectral type (and $B - R$) at -1.7 to -1.8 up to early M-type stars, when they increase rapidly to -1.3 at M5. We have found that 11 (17 per cent) of the 64 sources we have classified as coronal were emitting at a higher $\log(f_X/f_R)$ than predicted for a saturated source, 7 (11 per cent) by at least 0.5 dex (a factor of 3). If any ‘extragalactic’ and ‘no man’s land’ sources are actually coronal, most of these must also be emitting above their nominal saturated limits. This suggests that a significant proportion of our detected sources may be active coronae caught while flaring. This is reasonably consistent with the conclusions of Fleming et al. (1995) that approximately one quarter of solar-type stars and half of dMe stars in the EMSS were detected while flaring. Source 91 was actually seen to flare during the observation. It was undetected in the first half of the exposure time, but rose by a factor of at least 30 in ~ 15 ks to become the third brightest source in the survey. Its $\log(f_X/f_R)$ value increased from less than -1.0 , where it would fall into the coronal zone, to $+0.5$, where it climbs well into the extragalactic zone.

6 COMPARISON WITH MODELS OF CORONAL CONTRIBUTIONS TO X-RAY SOURCE POPULATIONS

Numerical models that predict the $\log N - \log S$ of stellar sources found in flux-limited X-ray surveys have been produced, based on Galactic structure models and the observed X-ray luminosity functions (XLFs) of various classes and ages of stars. Fig. 9 compares our observed number–flux relation for the hard band to those predicted by two such models. Such comparisons between these models and survey results can reveal irregularities in the local stellar formation rate (SFR) and inconsistency with the assumed spatial distribution of the sources, particularly the youngest stellar population, which is the most X-ray active, and particularly at low Galactic latitudes.

The *XCOUNT* model (Favata et al. 1992) is based on the Bahcall & Soneira Galactic structure model, and adopts different scaleheights for three age ranges of star (Micela, Sciortino & Favata 1993). *Einstein* IPC XLFs are used for each different age and spectral class of star. The Bahcall & Soneira model is derived from optical star counts, which are insensitive to the age distribution of the stellar population, whereas the X-ray source

counts are strongly dependent upon the number of young stars. Discrepancies between optical and X-ray counts are expected to be strongest near the Galactic plane, where the young stars are most concentrated. Even at high Galactic latitudes, an overabundance of ‘yellow’ X-ray emitting stars has been found (cf. Hodgkin & Pye 1994; Sciortino, Favata & Micela 1995), indicating the existence of a young local population not included in the standard Bahcall & Soneira model. It has thus been shown that X-ray counts can put useful constraints on the star formation rate (Micela et al. 1993).

We initially used the *XCOUNT* model for a constant SFR to predict the number of stellar sources in our survey region. In the PSPC hard band, for the total area of 2.5 deg^2 , we derived predictions for the $\log N - \log S$ curves for main-sequence (F–M) stars, giants and RS CVn’s. A large source of uncertainty exists due to the spatial density of RS CVn’s being poorly defined. The full range of densities obtained from Favata, Micela & Sciortino (1995) ($3.14 \times 10^{-5} - 1.22 \times 10^{-4} \text{ pc}^{-3}$) was used for the modelling. Following Micela et al. (1993) we derived a prediction of 22–31 ($9-13 \text{ deg}^{-2}$) stellar sources above $0.002 \text{ count s}^{-1}$. This is approximately half the 44–54 (69–85 per cent of the 64 hard sources detected in our survey) sources with count rate $> 0.002 \text{ count s}^{-1}$ that are coronal following our classification. The relative contribution of each stellar population to the predicted number of X-ray sources is shown in Table 6.

This shows that a constant stellar birthrate *XCOUNT* model underpredicts the coronal contribution to the $\log N - \log S$ on the Galactic plane. However, the *XCOUNT* predictions can be reconciled with our observations by assuming that the stellar birthrate has doubled during the last billion years, without any changes on the scaleheights. Under this assumption, leaving unchanged the contribution of active binaries, the *XCOUNT* model predicts 36–44 ($14-18 \text{ deg}^{-2}$) coronal sources that compare better with the observed number of coronal sources. We note that such a change in the stellar birthrate is not unrealistic since it would increase only by 10 per cent the total number of stars in the Galaxy, for an age of the old stellar population in the range $1-10 \times 10^9$ yr, with a small effect on optical number counts.

In the soft band *XCOUNT* predicts 2–3 stellar sources above $0.0025 \text{ count s}^{-1}$ for a constant SFR, and 3–4 in the case of a doubling of the SFR in the last billion years. These numbers compare well with the 4–5 likely coronal sources (cf. Tables 3 and 4) out of the 11 detected in the soft band above the limiting rate ($0.0025 \text{ count s}^{-1}$) corresponding to 90 per cent completeness of our survey.

Guillout et al. (1996a) have produced a model based on their Besançon evolution synthesis model which self-consistently computes the variation of scaleheight with age, assuming a constant SFR. As in *XCOUNT*, a similar three age ranges are defined, within which each spectral class has its own XLF. The more recent *ROSAT* PSPC XLFs are used for most classes. The scaleheight of the two younger populations is approximately half that applied in *XCOUNT*, and hence the density on the Galactic plane is almost doubled. In order to make a comparison with our observation, we have used the results in table 4 of Guillout et al. (1996a), which however are computed in the *ROSAT* broad-band (0.1–2.4 keV). Since, for a source of a given X-ray luminosity, the broad-band count rate is higher than the hard-band count rate, we have to ‘rescale’ the Guillout et al. results into the hard band. The rescaling is however spectrum-dependent; assuming emission from a single-temperature coronal plasma with $\log T = 0.7$ and $N_H = 2 \times 10^{20}$, a hard rate of $0.0020 \text{ count s}^{-1}$ will translate into a broad rate of $0.0025 \text{ count s}^{-1}$, while for the same temperature

and $N_{\text{H}} = 4 \times 10^{20}$, a hard rate of $0.0020 \text{ count s}^{-1}$ will translate into a broad rate of $0.0022 \text{ count s}^{-1}$. Scaling the Guillout et al. results on the basis of the above considerations, we predict about 16 and 17.3 coronal sources per square degree. Predicted coronal source numbers tend to decrease with the softening of the source spectrum, because of the different bandpass.

Thus the Besançon model with a constant SFR produces results that are similar to those obtained with XCOUNT doubling the SFR in the last billion years, and both models have similar ability to reproduce the source counts found in our surveys. However, the Besançon model prediction does not include a population of RS CVn-like binaries, which could provide a significant contribution to the coronal $\log N$ - $\log S$ in the Galactic plane (cf. Fig. 9).

While our data allow us to conclude that the density of young stars in the plane is higher than previously thought (e.g. Basu & Rana 1992), they alone cannot constrain the scaleheight of the young stellar population. The increase of young star density is supported by recent discoveries of nearby young stellar associations through *Hipparcos* proper-motion measurements (e.g. Tucanae Association, $\sim 10 \text{ Myr}$, at 50 pc; Zuckerman & Webb 2000) and through identification of X-ray sources (e.g. Horologium Association, $\sim 30 \text{ Myr}$, at 60 pc; Torres et al. 2000), which suggest that there has been an increase in the SFR in the solar neighbourhood in the last 10–100 Myr. The Gould Belt structure also suggests a recent, local ‘large-scale’ episode of star formation (Guillout et al. 1998). Based on our results we can rule out the cases in which the young stellar population is characterized either by large scaleheight *and* constant SFR (underpredicting the number of coronal sources) or small scaleheight *and* higher local mean SFR in the last billion years (overpredicting the number of coronal sources) – the first case being the ‘standard’ XCOUNT discussed above, the second one being the Besançon model with an increasing SFR (Guillout et al. 1996b). Hernandez, Valls-Gabaud & Gilmore (2000) have used *Hipparcos* data to show that the local SFR may be episodic, rather than following a continuous trend.

7 SUMMARY

We have performed a soft X-ray survey of the Galactic plane that is more than an order of magnitude deeper than previous X-ray surveys near the Galactic plane. A sky area of 2.5 deg^2 was surveyed, yielding 93 sources, 64 with hard-band (0.4 – 2.0 keV) fluxes $> 2 \times 10^{-14} \text{ erg cm}^{-2} \text{ s}^{-1}$. On the basis of $\log(f_{\text{X}}/f_{\text{opt}})$ versus optical colour diagrams (USNO-A2.0 and Tycho-2) and near-IR photometry (2MASS), we found 69 per cent of the sources to have counterparts consistent with being coronal sources, with 15 per cent consistent with extragalactic sources, 10 per cent inconsistent with either of these two classes, 4 per cent to be early-type stars or H II regions, and 1 per cent to have no nearby optical or near-IR counterpart ($R \leq 19$, $J \leq 16$).

These results are in agreement with conclusions from earlier high-flux X-ray surveys in the plane, such as the EGPS and the RGPS, that the majority of sources are consistent with late-type stars, and indicate that active coronae remain the dominant population of X-ray sources more than an order of magnitude fainter in flux than the sensitivity limits of previous studies.

A significant percentage (10–20 per cent) of ‘coronal’ sources were detected while emitting above their nominal saturated limit [$\log(L_{\text{X}}/L_{\text{bol}}) = -3$], consistent with Fleming et al.’s (1995)

conclusion that 25 per cent of solar-like stars and 50 per cent of dMe stars were detected while flaring.

Our data allow us to rule out models of stellar X-ray counts in which the young stellar population is characterized either by large scaleheight *and* constant SFR or small scaleheight *and* increased SFR in the last billion years. The observed count can be equivalently explained with the XCOUNT model by assuming an SFR doubled in the last billion years and including the contribution of active binaries, or with the Besançon model with a constant SFR but without including the contribution of active binaries, which, on the other hand, could provide a significant contribution to the coronal number count in the Galactic plane.

Our results support the view that the population of young stars in the plane is denser than previously thought, and highlight the ability of flux-limited X-ray surveys to map the young stellar component of the Galaxy.

ACKNOWLEDGMENTS

JEM, JPP and KRB acknowledge the financial support of the UK Particle Physics and Astronomy Research Council (PPARC). This work made use of archival material from the SIMBAD and VIZIER systems at CDS, Strasbourg, and the Leicester Database and Archive Service (LEDAS). SS and GM acknowledge support from the Italian Space Agency (ASI) and Ministero della Ricerca Scientifica e Tecnologica (MURST).

REFERENCES

- Allan D. J., 1992, ASTERIX User Note 004, Starlink, Rutherford Appleton Laboratory
 Allen C. W., 1973, *Astrophysical Quantities*. 3rd edn. Athlone, London, p. 1973
 Ayres T. R., Linsky J. L., Vaiana G. S., Golub L., Rosner R., 1981, *ApJ*, 157, 1157
 Bahcall J. N., Soneira R. M., 1980, *ApJS*, 44, 73
 Bahcall J. N., Soneira R. M., 1984, *ApJS*, 55, 67
 Basu S., Rana N. C., 1992, *ApJ*, 393, 373
 Belloni T., Mereghetti S., 1994, *A&A*, 286, 935, (BM94)
 Bessell M. S., Brett J. M., 1988, *PASP*, 100, 1134
 Boyle B. J., McMahon R. G., Wilkes B. J., Elvis M., 1995, *MNRAS*, 276, 315
 Branduardi-Raymont G. et al., 1994, *MNRAS*, 270, 947
 Briggs K. R., Pye J. P., Jeffries R. D., Totten E. J., 2000, *MNRAS*, 319, 826
 Bronfman L., Nyman L., May J., 1996, *A&AS*, 115, 81
 Cohen M., Jones B. F., Walker H. J., 1989, *ApJ*, 341, 908
 Cutri R. M. et al., 2000, <http://www.ipac.caltech.edu/2mass/>
 Dame T. M. et al., 1987, *ApJ*, 322, 706
 ESA, 1997, *The Hipparcos and Tycho Catalogues*, ESA SP-1200, 1-17. ESA Publications Division, Noordwijk
 Favata F., Micela G., Sciortino S., Vaiana G. S., 1992, *A&A*, 256, 86
 Favata F., Micela G., Sciortino S., 1995, *A&A*, 298, 482
 Finlator K. et al., 2000, *AJ*, 120, 2615
 Fleming T. A., Molendi S., Maccacaro T., Wolter A., 1995, *ApJS*, 99, 701
 Frisch P. C., York D. G., 1983, *ApJL*, 271, 59
 Guillout P., Haywood M., Motch C., Robin A. C., 1996a, *A&A*, 316, 89
 Guillout P., Haywood M., Motch C., Robin A. C., 1996b, in Zimmermann H. U., Trümper J., Yorke H. eds, *Proc. Röntgenstrahlung from the Universe*. MPE Report 263, p. 41
 Guillout P., Sterzik M. F., Schmitt J. H. M. M., Motch C., Neuhauser R., 1998, *A&A*, 337, 113
 Haberl F., Pietsch W., 1999, *A&AS*, 139, 277
 Haberl F., Filipović M. D., Pietsch W., Kahabka P., 2000, *A&AS*, 142, 41
 Haisch B. M., Simon T., 1982, *ApJ*, 263, 252

⁹The direction of the present survey is largely outside the Gould Belt structure discovered by Guillout et al. (1998); only field 9 lies within it.

- Hasinger G., Burg R., Giacconi R., Hartner G., Schmidt M., Trümper J., Zamorani G., 1993, *A&A*, 275, 1
- Hernandez X., Valls-Gabaud D., Gilmore G., 2000, *MNRAS*, 316, 605
- Hertz P., Grindlay J. E., 1984, *ApJ*, 278, 137
- Hertz P., Grindlay J. E., 1988, *AJ*, 96, 233
- Hodgkin S. T., Pye J. P., 1994, *MNRAS*, 267, 840
- Høg E. et al., 2000, *A&A*, 355, L27
- Humphreys R. M., Landau R., Ghigo F. D., Zurnach W., Labonte A. E., 1991, *AJ*, 102, 395
- Johnson H. L., 1966, *ARA&A*, 4, 193
- Lampton M., Margon B., Bowyer S., 1976, *ApJ*, 208, 177
- Machalski J., Wiśniewski W. Z., 1988, *MNRAS*, 231, 1065
- Micela G., Sciortino S., Favata F., 1993, *ApJ*, 412, 618
- Monet D. et al., 1998, *USNO-Av.2.0, A Catalogue of Astrometric Standards*. US Naval Observatory Flagstaff Station
- Morley J., 1998, PhD thesis, Univ. Leicester
- Motch C. et al., 1991, *A&A*, 246, 24
- Motch C., Guillout P., Haberl F., Pietsch W., Reinsch K., 1997, *A&A*, 318, 111
- Motch C. et al., 1998, *A&AS*, 132, 341
- Palagi F., Cesaroni R., Comoretto G., Felli M., Natale V., 1993, *A&AS*, 101, 153
- Paresce F., 1984, *AJ*, 89, 1022
- Pfeffermann E. et al., 1986, *Proc. SPIE*, 733, 519
- Schmidt-Kaler Th., 1982, *Landolt-Börnstein Numerical Data and Functional Relationships in Science and Technology, New Ser., Group IV, Vol. 2b, Physical Parameters of the Stars*. Springer-Verlag, Berlin
- Sciortino S., Favata F., Micela G., 1995, *A&A*, 296, 370
- Seeberger R., Saurer W., Weinberger R., 1996, *A&AS*, 117, 1
- Stark A. A., Gammie C. F., Wilson R. W., Bally J., Linke R. A., Heiles C., Hurwitz M., 1992, *ApJS*, 79, 77
- Stocke J. T., Morris S. L., Gioia I. M., Maccacaro T., Schild R., Wolter A., Fleming T. A., Henry J. P., 1991, *ApJS*, 76, 813
- Torres C. A. O., da Silva L., Quast G. R., de la Reza R., Jilinski E., 2000, *AJ*, 120, 1410
- Trümper J. et al., 1991, *Nat*, 349, 579
- Zuckerman B., Webb R. A., 2000, *ApJ*, 535, 959

This paper has been typeset from a \TeX/L\AA\TeX file prepared by the author.